Phylogeny indicates polyphyly in *Cnodocentron* (Trichoptera: Xiphocentronidae): biogeography, status elevation and revision of the New World species

Cnodocentron has a disjunct laurasian distribution, with species in Southeastern Asia and New World separated into different subgenera, *Cnodocentron* and *Caenocentron*. Here, we infer the evolutionary history of the genus through phylogenetic and biogeographic data combining COI and 46 morphological characters. Phylogenetic relationships and divergence time estimation were simultaneously inferred through Bayesian analyses. The dating analysis was performed through relaxed morphological and molecular clocks. The historical biogeography was investigated through the Dispersal–Extinction–Cladogenesis model. Our results indicated the polyphyly of the genus *Cnodocentron*, each subgenus being more related to other genera from the same biogeographic region than to each other. Therefore, the subgenus *Caenocentron* was elevated to generic status. The biogeographical analysis showed that the Oriental *Cnodocentron* diverged in the Indian subcontinent during the Middle Eocene, while the New World *Caenocentron* **stat. nov.** originated in the Chortis block in the Late Eocene. The dispersal of *Caenocentron* to South America occurred only after the Late Miocene around 10 Mya. Additionally, we provide a revision of the species of *Caenocentron* **stat. nov.**, with identification key and description of the male and female of two new species from Costa Rica: ***Caenocentron carlosdelarosai* sp. nov.** and ***Caenocentron rafamoralesi* sp. nov.**

ADDITIONAL KEYWORDS: Insecta - bayesian analysis - identification key - new species - biogeography - revision - taxonomy

INTRODUCTION

The Xiphocentronidae Ross, 1949 are a rare net-tube caddisfly family that originated in the early Cretaceous around 130 Mya (Malm *et al.*, 2013; Thomas *et al.*, 2020). During this period, the climate was much warmer and wetter than today, with the poles free of ice and arctic ocean temperatures around 20ºC (Hay, 2017; Jenkyns *et al.*, 2004). Currently, the xiphocentronids are mostly restricted to warm regions, with 193 species and seven genera distributed throughout the tropics (Fig. 1) (Vilarino & Bispo, 2020; Morse 2021). Among the genera of the family, *Proxiphocentron* Schmid, 1982; *Drepanocentron* Schmid, 1982; *Melanotrichia* Ulmer, 1906 and *Abaria* Mosely, 1948 occur mainly in the Oriental region. *Xiphocentron* Brauer, 1870 and *Machairocentron* Schmid, 1982 are mainly Neotropical. The genus *Cnodocentron* Schmid, 1982 (13 spp.) is the only one to occur simultaneously in the Oriental region and New World (mainly Neotropics) (Vilarino & Bispo, 2020). Based on the diversity and present distribution of the family, Schmid (1982) suggested that the xiphocentronids have an Oriental origin, with the dispersal to the Americas occurring through the Bering land bridge during the Eocene hyperthermal events; however, this hypothesis was never properly investigated. Therefore, *Cnodocentron,* with its disjunct distribution, can be a good model to shed light on the biogeography of the family.

The genus *Cnodocentron* was established by Schmid (1982) based on the male genitalia presenting bifurcate inferior appendages. The genus was classified into two subgenera: *Cnodocentron* (*Cnodocentron*) (currently with six spp.) present in the Oriental region (India, Thailand, and Vietnam); and *Cnodocentron* (*Caenocentron*) (currently with seven spp.) present in the New World (from the southwestern USA to northern South America, including USA, Mexico, Guatemala, El Salvador, Nicaragua, Costa Rica, Panama, and Colombia) (Fig. 1) (Morse, 2021). The adults of the two subgenera can be easily distinguished by the male genitalia and wing pattern. The preserved pinned specimens of the subgenus *Caenocentron* have forewings with three transverse patches of white setae, while the specimens of subgenus *Cnodocentron* have only a single white patch, although, this color pattern usually fades away in the specimens preserved in alcohol.

The adults of *Cnodocentron,* as other Xiphocentronidae, actively fly during the daytime (Schmid, 1982; Flint, 1981) and are rarely collected through light traps (Moulton & Stewart 1997). Since the establishment of the genus, only three new species were described, two Oriental species (*C. brogimarus* Malicky & Chantaramongkol, 1992; C. *filamenta* Oláh & Johanson, 2010), and one Nearctic species (*C. yavapai* Moulton & Stewart, 1997). The larva, pupa (Moulton & Stewart 1997), and the female (Ruiter, 2006) were described only for *C.* (*Caenocentron*) *yavapai.* Schmid (1982) mentioned some female allotypes, but they were not described. The larva is similar to other xiphocentronids, building retreats over partially submerged rocks and feeding on diatoms (Moulton & Stewart, 1997). The pupa differs from other known xiphocentronids by the posterior margin of tergum VII with a dense fringe of setae (Moulton & Stewart, 1997).

Although the proposition of the genus was made almost 40 years ago, the monophyly of the genus, subgenera, and their relationship has never been tested. In addition to testing the monophyly, a time-calibrated phylogeny would make it possible to test the hypothesis of intercontinental dispersal between Asia and America during the Eocene, and to understand the diversification and biogeography of the genus. The recent application of relaxed morphological clock in Bayesian inference makes it an important tool for estimation of divergence times from morphological data. The relaxed morphological clock has been used in total-evidence dating methods (including molecular and morphological data) (*e.g.,* Pyron, 2011; Ronquist *et al*., 2012a) as well as in tip-dating methods, using morphological data only (*e.g.,* Lee *et al.*, 2014; Close *et al.*, 2015; Wright, 2017; Lucena & Almeida, 2021). This approach allows the inclusion of a time dimension to phylogenies of fossil and living groups with little or no molecular data available, as is the case of the Xiphocentronidae. The incorporation of time adds much more explanatory power to the evolutionary inferences, since the hypothesis of the biogeographic events associated with each cladogenesis can be tested with more accuracy (Sanmartín, 2012).

Here, we studied the specimens of *Cnodocentron* and proposed a phylogeny aiming to 1) test the monophyly of the genus and the two subgenera; 2) test the hypothesis of intercontinental dispersal through the Bering land bridge during the Eocene (Schmid, 1982); and 3) infer the first biogeographical hypothesis for the

diversification of *Cnodocentron* in the Southeast Asia and New World. Additionally, we revise the New World species, describing two new species based on males and females, and providing an identification key.

MATERIAL AND METHODS

MORPHOLOGICAL TERMINOLOGY, SPECIMENS PREPARATION, AND ILLUSTRATIONS

The following terminologies were used in this study: 1) male genitalia, modified terminology from Nielsen (1957) and Schmid (1982); 2) female genitalia, modified from Nielsen (1980); 3) head setal warts, modified from Oláh & Johanson (2007); 4) wing venation, Comstock – Needham system as interpreted for Trichoptera by Mosely & Kimmins (1953). Paired structures were referred to in the singular form in the descriptions. The wings were mounted on slides to study the venation following standard protocols outlined by Prather (2003). The genitalia were studied after removing and diaphanizing the specimen's abdomen using 85% lactic acid through standard methods outlined by Blahnik et al. (2007). The prepared genitalia samples were transferred to microvials with 80% ethanol, and later were placed in depression slides with a drop of glycerin and examined using a compound microscope (Olympus BX41) at 400X magnification. The genitalia of some Schmid's (1982) type specimens were fixed in a permanent slide and displayed in lateral view. These species were re-illustrated only in lateral view to avoid damaging the holotypes, in cases when additional specimens were not available. Phallus structure is mostly the same in all species and was only depicted to *Cnodocentron (Caenocentron) trilineatum* (Mosely, 1934). The illustrations of the structures were traced with pencil using a drawing tube coupled to the microscope, and the scanned pencil drawings were digitally traced on the computer using Adobe Illustrator® CS6. The left preanal appendage was omitted in some illustrations to allow the visualization of the inferior appendage. Photographs of different parts of the specimens were taken using a Leica Camera (DFC450) coupled to a Leica stereomicroscope (M2020) and edited with Adobe Illustrator® CS6. The distribution maps were generated using the opensource software QGIS version 2.8.2, and geographical data was compiled from original descriptions and checklists.

PHYLOGENETIC ANALYSES

Taxa included in the phylogenetic analyses are presented in Table 1. The ingroup included all the 15 *Cnodocentron* species (including the new species described here). The outgroups included ten species representatives of three genera: *Drepanocentron vang* Oláh & Johanson, 2010; *Melanotrichia attia* Malicky & Chantaramongkol, 1992; *M. attiaides* Mey, 1998; *M. samaconius* Malicky & Chantaramongkol, 1992; *X.* (*Antillotrichia*) *haitiensis* (Banks, 1941); *X.* (*Antillotrichia*) *maiteae* Vilarino & Calor 2015; *X.* (*Antillotrichia*) *mnesteus* Schmid, 1982; *X.* (*Glyphocentron*) *euryale Schmid, 1982*; *X.* (*Rhamphocentron*) *messapus* Schmid, 1982; and *X.* (*Xiphocentron*) *aureum* Flint, 1967.

The final phylogenetic dataset comprised 25 taxa (15 ingroup taxa, ten outgroup) with 46 morphological characters (Table 2) and sequences of cytochrome oxidase I (COI) available for eight terminals (Table 3). Morphological characters and character state constructions were based on Sereno (2007). When a given structure was not present in the analyzed specimens, it was coded as '-'; when the character state was not clear or could not be assessed, it was coded as '?'. Most of the characters were binary (40), and all multistate characters (6) were treated as unordered. Characters were coded from literature rather than direct observation for (4 species): *Cnodocentron ideolus* Schmid, 1982; *C. girika* Schmid, 1982; *C. filamenta* Oláh & Johanson, 2010; and *C. devayani* Schmid, 1982. The morphological dataset matrix was built using the software Winclada 1.89 (Nixon 2002).

The phylogeny was based on a probabilistic framework through Bayesian inference as implemented in MrBrayes 3.2.7 (Ronquist *et al.*, 2012b). The morphological dataset was analyzed using the Mk model (Lewis, 2011). To adjust the heterogeneity in rates of evolution across morphological characters, we adopted a homoplasy-based partitioning strategy described by Rosa *et al.* (2019), which was shown to outperform other approaches for modeling among character rate variation. In the homoplasy-based approach, the levels of character compatibility are estimated from the relative homoplasy calculated from the consistency index generated in an implied weights parsimony analysis. The parsimony analysis was performed in TNT version 1.1 (Goloboff *et al.*, 2008). Heuristics searches were performed through 'Traditional Search', with $2x10^4$ replications, five trees saved per replication. The characters were

analyzed under Self-Weighted optimization (weighting state transformations), using default settings (Goloboff, 1997). Despite being more time-consuming, weighting state transformations is interesting due to its higher sensitivity to parallelism events, where character transformations in one direction are more common than in another (Molineri, 2006; Mirande, 2009). Since we only aimed to segregate the characters according to homoplasy intervals, we used the default value for concavity constant (K=3). The adjusted values of homoplasy (consistency index) of each character were combined into more inclusive intervals resulting in seven partitions (Table 4). These morphological character partitions were then used in the Bayesian analyses.

The COI sequences available in the BOLD website (Barcode of life Database) were included to provide additional information about branch lengths and relationships among the genera. We included in the phylogenetic analyses COI sequence fragments for eight species (Table 3). The sequences were aligned using MAFFT through the method L-INS-I (Katoh & Standley, 2013), partitioned by codon position, and concatenated with the morphological dataset in SequenceMatrix 1.8 (Vaidya *et al.*, 2011). The CO1 evolution models were estimated to each codon position using J-ModelTest 2 (Darriba *et al.*, 2012), followed by the selection of the models: GTR+G, HKY, and HKY+G, respectively; and the analysis of each partition with unlinked parameters.

DIVERGENCE TIMES ESTIMATION

The divergence times were generated together with the phylogenetic analyses in Mrbayes 3.2.7 as detailed by Zhang (2019). We used a node dating calibration with a relaxed clock and a constrained prior for the root. The tree was rooted in *Drepanocentron* and calibrated according to the age inferred in the fossil calibrated phylogeny proposed by Malm *et al.* (2013) (*i.e.,* mean age 68.74 Mya) (*offsetlognormal (49,68.74,18)*). The fossil of *X.* (*Xiphocentron*) *chiapasi* Wichard *et al.*, 2006 from Miocene (16–23 Mya) was used to calibrate the node of *X.* (*Xiphocentron*) *aureum* (*offsetexp (16,20)*). We assigned a root constraint to *Drepanocentron,* and a monophyly constraint for the fossil calibrated node.

We used two independent relaxed clocks, one to the morphological characters and one to the COI, both using the independent gamma rate (IGR) model (*prset*

clockvarpr = igr) (Lepage *et al.*, 2007). The clock rates priors were linked for CO1 partitions and unlinked for morphological partitions. For the clock rate prior, we used a lognormal distribution adjusted according to the rootage as 1/68.74 (one change by the mean age of root prior of the tree) = 0.0145 changes per million years. This value was set as the substitution rate, with mean log value μ = -4.355 and standard deviation σ = 0.5 (*prset clockratepr = lognorm(-4.355, 0.5)*). We used the birth-death prior under diversified sampling (Höhna *et al*., 2011) to model the time-calibrated trees. We followed the same priors proposed by Zhang *et al.* (2016) for the diversification sampling. To obtain a proportional sampling of living groups (*prset sampleprob*), we calculated the number of terminals included in the analysis by the approximate number of Xiphocentronidae species (25 terminals by approximately 200 species = 0.125). We adopted the diversity strategy for the sampling of species (*prset samplestrat*).

The analyses were performed through the CIPRES gateway (Miller *et al.*, 2010) for 5×10^7 generations in 2 parallel analyses and 4 Markov chains, and the initial 25% generations were discarded as burn-in. We checked the convergence among the analyses in Tracer 1.7 (Rambaut *et al.*, 2018). The maximum credibility Bayesian tree was calculated in MrBayes with all compatible groups allowed (*contype = allcompat*). The branch support was measured by the posterior probability values. The trees were visualized and edited in FigTree 1.4.3 (Rambaut, 2016) and in Winclada 1.89 (Nixon, 2002), the final phylogeny was edited in Adobe Illustrator® CS6.

BIOGEOGRAPHIC ANALYSIS

The distribution range of the species was divided into eight areas based on tectonic provinces of Mesoamerica (Dengo, 1985) and Asia (Hall, 2012): (a) Nearctic region; (b) Mexican transition zone; (c) Maya block; (d) Chortis block; (e) Chorotega block; (f) Antilles; (g) South America; (h) Southeast Asia; and (i) Indian plate. The distributional data were obtained through the material analyzed (recorded from specimen's labels) and from the literature. We inferred the historical biogeography of *Cnodocentron* through event-based models. The models fit to the data were compared using likelihood-ratio test and AIC through the package BioGeoBEARS (Matzke, 2014). The Dispersal–Extinction–Cladogenesis model (DEC) (Ree & Smith, 2008) was selected as the best fit model. The DEC ancestral range estimation was implemented in RASP version 4.0

(Reconstruct Ancestral State in Phylogenies) (Yu *et al.*, 2020). The analyses were run on a pruned tree obtained from the maximum credibility Bayesian dated tree. The area corresponding to the Chorotega block was time stratified, being allowed only after the early Miocene (~22 Mya) according to fossil and stratigraphic evidence of terrestrial connection (Kirby *et al.*, 2008). In the analyses, the maximum number of combined areas to each node was set to five, with no range constraints. The biogeographic events associated to each node (*i.e.,* dispersal, vicariance) were inferred by the analysis in RASP. The biogeographic results were displayed showing most likely states only and edited using Adobe Illustrator CS6.

DNA BARCODE AND MALE-FEMALES ASSOCIATION

The mitochondrial COI sequence fragments (DNA barcode) for several Xiphocentronidae species, including the two new species described here, were previously available at the BOLD website (Barcode of Life Database) as unidentified species, which were identified in this study. The sequences were used to associate males and females of the new species. The females and males were considered as the same species when they were clustered in the same monophyletic clade, following a Phylogenetic Species Concept (Eldredge & Cracraft, 1980). To associate male and female specimens, the COI sequences of the *Cnodocentron* (*Caenocentron*) and other xiphocentronids available at BOLD were aligned as detailed in the phylogenetic analyses section. The GTR+I+G evolution model was selected using the J-ModelTest, and the Bayesian analyses were implemented in MrBayes. The analyses were performed following the same procedures detailed in Divergence Times Estimation section. Intra and interspecific genetic distances were computed using the Kimura 2-parameter (K2P) model (Kimura, 1980) in the software Mega X (Kumar *et al.*, 2018).

DEPOSITORIES

Types of the species described herein, and other material examined are deposited, as indicated in each species description and in the Table 1, in the following institutions. BIOUG – Centre for Biodiversity Genomics, University of Guelph, Ontario, Canada; CNC – Canadian National Collection of Insects, Arachnids, and Nematodes, Ottawa, Canada; MZSP – Museu de Zoologia, Universidade de São Paulo, São Paulo, Brazil;

USNM – U.S. National Entomological Collection, Smithsonian Institution, Washington, DC, USA; UMSP – University of Minnesota Insect Collection, Saint Paul, Minnesota, USA.

RESULTS

CHARACTERS AND STATES FOR CLADISTIC ANALYSIS

The morphological characters and their respective states obtained from the study of the specimens and/or literature are listed below. The resulting matrix is presented in Table 2

Female character

1. *Female, abdominal segment viii, setae shape*: (0) seta with same overall width (Fig. 4M); (1) seta base distinctly thickened (Fig. 4N).

Adult characters

2. *Mesoscutelum, lateral edges shape*: (0) edges straight (Fig. 3B, 3D); (1) edges rounded (Fig. 3A, 3C).
3. *Hind leg, apical spur aspect*: (0) similar to other spurs (Fig. 3F); (1) distinct from spurs of other legs (distinctly enlarged and\or twisted) (Fig. 3E).
4. *Abdominal sternum V anterior margin, pair of reticulated sclerotized cuticular plates*: (0) absent (a small papilla might be present around the glandular opening, Fig. 2D); (1) present, (broad reticulated plates present, Fig. 2B, C).

Wing characters

5. *Hindwing, transverse vein between R1 and SR (consider here homologous to R2+3)*: (0) absent (Fig. 4A, 4C); (1) present (Fig. 4B).
6. *Forewing, fork II nygma*: (0) not surrounded in a vein cell (Fig. 4C); (1) surrounded in a vein cell (Fig. 4B).
7. *Forewing, fork II (R4 + R5)*: (0) sessil (Fig. 4C); (1) petiolate (Fig. 4B).
8. *Forewing, apex shape*: (0) acute (Fig. 4A-C); (1) rounded (Fig. 7B).
9. *Forewing, Sc*: (0) ending at the wing margin (Fig. 4C); (1) looping in R1 before reaching wing margin.
10. *Forewing, color pattern*: (0) without spots or with one spot; (1) with 3 white spots (Fig. 2A).

Male genitalia characters

11. *Sternum IX, apodeme shape*: (0) broad, contiguous with anterior margin (Fig. 4E, F); (1) narrow, finger-like, angulate to anterior margin (Fig. 8A).
12. *Sternum IX, apical margin*: (0) sternum margin without apical structures (Fig. 8C); (1) with projections or spines fused to sternum margin (Fig. 4G-L, 13D, 14C).
13. *Sternum IX, projection type*: (0) two processes (fused to each other or not) (Fig. 4G-I); (1) multiple stout spines/processes (Fig. 4J-L).
14. *Sternum IX, projection sutures*: (0) fused with sternum without sutures (Fig. 4G, 4J); (1) connected to sternum margin but with distinct suture lines (Fig. 4H-I).
15. *Sternum IX apical margin, lateral projection*: (0) absent (Figs 4E-F, 4J-L); (1) present (Fig. 4G-I).
16. *Sternum IX, dorsal margin (in lateral view)*: (0) straight (Fig. 14A); (1) produced dorsad (Fig. 8A).
17. *Sternum IX, incision near preanal appendage*: (0) absent (Figs 8A, 13B); (1) present (Fig. 4E, F).
18. *Tergum IX, shape*: (0) reduced, or membranous (Figs 13C, 14B); (1) elongate, with apical lobes (present in some *Xiphocentron* and some *Melanotrichia*).
19. *Paraproct, ventral process*: (0) absent; (1) present (Fig. 16A).
20. *Paraproct, lateral spines/setae*: (0) absent; (1) present (Fig. 19C, 20C).
21. *Paraproct, dorsal process (in lateral view)*: (0) absent (fused to dorsal band); (1) present (Fig. 8A).
22. *Preanal appendage, width (in lateral view)*: (0) distinctly slender most of its length (Figs 8A, 13B, 15A); (0) broader width most of length (Figs 4E-F, 14A).
23. *Preanal appendage, longitudinal ridge*: (0) absent; (1) present (Fig. 4E).
24. *Preanal appendage, shape*: (0) straight, to slightly undulate; (0) markedly sigmoid (subbasally bent).
25. *Inferior appendage, coxopodite and harpago fusion*: (0) broadly fused; (1) segments well distinct by suture.
26. *Basal plate apodeme, length*: (0) short (Fig. 19D, 20D); (1) elongate (Figs 13D, 14C); (2) very elongate (Fig. 4E-F).

27. *Basal plate apodeme, apex direction*: (0) anterad (Fig. 4E, F); (1) ventrad (Figs 19B, 20B).
28. *Coxopodite, basoventral margin*: (0) without any projection (Fig. 4E-F); (1) with projection (Fig. 8A, 13B).
29. *Coxopodites, basoventral margin projection*: (0) each projection separated (Fig. 13D); (1) projection fused to each other (Fig. 8C).
30. *Coxopodite, ventral projection pair of stout spines*: (0) absent (Fig. 8A, 8C); (1) present (Figs 15A-B).
31. *Coxopodite, apical margi*n: (0) not produced (Fig. 4E); (1) produced posterad (Figs 4F, 8A).
32. *Coxopodite, apical margin projection degree*: (0) mild (less than 1/3 of harpago length); (1) markedly produced (reaching more than 1/3 of harpago length) (Fig. 8A).
33. *Coxopodite, basomesal setal brush*: (0) absent; (1) present (just a granulose area when setae are very short) (Figs 8A, 13B).
34. *Coxopodite, basomesal setae length*: (0) very short (as in *X. messapus*, *X. euryale*, *X. mnesteus* e.g.); (1) long (Figs 13D, 14D, 16B); (2) very long (Fig. 8A-B).
35. *Coxopodite, apical projection subapical spine*: (0) absent (Figs 15, 19); (1) present (Figs 8, 17, 18).
36. *Coxopodite, apical projection branch number*: (0) single; (1) two (Fig. 14A, C).
37. *Coxopodite, apical projection shape*: (0) broad (Figs 17A, 18A, 19B); (1) narrow (Figs 16A, 20B).
38. *Harpago, basal spine*: (0) absent; (1) present (8A-B).
39. *Mesal process/projection*: (0) absent; (1) present (Figs 4D, 4E, 19B).
40. *Mesal process, ornamentation*: (0) without ornamentation; (1) topped with spines or projections (Figs 4D, 4E, 19B).
41. *Mesal process, shape*: (0) lobular, brush like (Fig. 19B); (1) broad fan like (Fig. 4D); (2) acute point-like.
42. *Mesal process, position*: (0) between harpago and coxopodite, (1) subapical.
43. *Harpago, brush-like setae*: (0) absent; (1) present (Figs 4F, 19B).

44. *Harpago, setose area placement*: (0) setose area on the basal region only (Figs 16A, 17A, 18A); (1) setose area extending from the basal region to midlenght, or apex (Fig. 4F); (2) setose area on the subapical region only.
45. *Harpago, brush-like setae length*: (0) short (Fig. 13B); (1) elongate (Figs 4F, 16A, 18A).
46. *Harpago, brush-like setae coverage area*: (0) narrow (linear row of setae) (Figs 16A, 18A); (1) broad area of setae (Fig. 4E); (2) sparse setae (Fig. 13B).

PHYLOGENY

The maximum credibility Bayesian tree obtained from the morphological characters and COI (Fig. 5) recovered *Cnodocentron* as a polyphyletic genus. Each subgenus *Cnodocentron* (*Cnodocentron*) and *Cnodocentron* (*Caenocentron*) was considered monophyletic individually but not directly related to each other. Therefore, we propose the elevation of the New World subgenus *Caenocentron* to generic status, and the genus *Cnodocentron* would be restricted to the Oriental species only. Hereafter, we will refer to each of these clades just as *Caenocentron* and *Cnodocentron*. To allow the observation of the character states distribution on the resulting Bayesian topology, all the morphological characters were displayed in accelerated optimization (ACCTRAN) along the branches in the figure 5. Only the unambiguous synapomorphies are discussed below.

In our topology (Fig. 5), *Cnodocentron* was a sister group of *Melanotrichia.* The clade *Cnodocentron* + *Melanotrichia* was highly supported (posterior probability value, pp=97) and has the following synapomorphies: straight mesoscutelum edges (2:0); acute forewing apex (8:0); and coxopodite basomesal face without setal brush (33:0). The *Cnodocentron* monophyly (pp=75) was recovered with the synapomorphies: female segment VIII with thickened setae (1:1); coxopodite margin produced posterad (31:1); and presence of elongate setal brushes on harpago (45:1).

Cnodocentron split into two main clades. The clade (*C. devayani* (*C. girika* + *C. vrisaparvan*)) (pp=83) is supported by the sternum IX apical margin presenting multiple spines (13:1). Within this clade, *C. girika* is grouped with *C. vrisaparvan* by the character state: inferior appendage articles well distinct from each other (25:1). The

second clade (*Cnodocentron brogimarus* (*C. chaturbhuja* + *C. filamenta*)) was a strongly supported group (pp=100) with the synapomorphies: the presence of a cell around the forewing nygma (6:1); and elongated lateral processes on the sternum IX (15:1). *C. chaturbhuja* and *C. filamenta* are grouped by the character states: forewing fork I petiolate (7:1) and harpago with sparse setae (46:2).

Caenocentron was closely related to the New World *Xiphocentron* included in the analysis (Fig. 5). The clade placing *Xiphocentron aureum* + *X. messapus* with other species of *Xiphocentron* + *Caenocentron* was highly supported (pp=100) but only based on COI. The clade grouping *Caenocentron* and some species of *Xiphocentron* (pp=99) was supported by the synapomorphies: presence of reticulate cuticular plates on sternum V (4:1), and preanal appendage sigmoid (24:1). The monophyly of *Caenocentron* was strongly supported (pp=100) with five synapomorphies: basal plate apodeme with apex directed ventrad (27:1); coxopodite basoventral margin produced (28:1); coxopodite apical margin produced (31:1); and harpago basal spine present (38:1).

The earliest splitting *Caenocentron* taxa, *C. rafamoralesi* **sp. nov.** and *C. yavapai,* were grouped together by presenting broader sternum IX apodemes (11:0) (pp=73). This clade was placed as a sister group to all other *Caenocentron*. In these two species, the sternum IX does not exhibit the typical structure of other *Caenocentron*; as the ventral projection of coxopodite is not very developed. The sister clade including all other *Caenocentron* was strongly supported (pp=100) based on the synapomorphies: sternum IX dorsal margin produced (16:1); paraproct with a distinct dorsal process (21:1); coxopodite and harpago well distinct (25:1); and basal plate apodeme very short (26:0); harpago brush placed basally (44:0); and harpago brush with long setae (45:1).

Other inferred cladogenetic events within this group should be intepreted with caution due to the low support values (pp<50), and fewer or no morphological synapomorphies supporting the clades (Fig. 5). The cladogenesis of *C. ideolus* and *C. trilineatum* (pp=46) is supported by the synapomorphy presence of lateral spines on the paraproct (20:1). The clade including (*C. pallas* (*C. immaculatum*, *C. galesus*) was the only one with high support (pp=76), all sharing a pair of stout spines on the ventral projection of coxopodite (30:1) as a unique synapomorphy. The clade (*C. carlosdelarosai* **sp. nov.**, *C. lausus*) had no morphological synapomorphies (pp=38),

their placement as a sister group of (*C. pallas* (*C. immaculatum*, *C. galesus*) also had no morphological support (pp=22) (Fig. 5).

BIOGEOGRAPHY AND DIVERGENCE TIMES ESTIMATION

Cnodocentron occurs in the Oriental region, with species from the eastern part of the Southern Himalayan flank and Southeast Asia highlands (East India, Thailand, and Vietnam). *Caenocentron*, in turn, occurs in the New World, with species ranging from the northwest of Colombia, passing through Central America to the southwest of the USA. The divergence between the New World clades (*Caenocentron* + *Xiphocentron*) and Oriental clades (*Cnodocentron* + *Melanotrichia*) is estimated with a mean age of 56.4 Mya coinciding with the Paleocene-Eocene thermal maximum (Fig. 6).

According to the biogeographical analysis (Fig. 6), *Cnodocentron* and *Melanotrichia* diverged during the middle Eocene (40.6 Mya), with the dispersal of *Cnodocentron* ancestors from Asia mainland to the Indian plate (Fig. 6). The divergence of the two main *Cnodocentron* clades, one in the Indian subcontinent and the other also present in the Southeast Asia, occurred during the Oligocene (29.9 Mya). While the clade from the Indian subcontinent remained restricted to this area, the clade from Southeast Asia dispersed between the two regions during the Middle Miocene (14.8 Mya), with a subsequent vicariant event between *C. filamenta* and *C. chaturbhuja* species occurring in the Late Miocene (9.0 Mya).

Caenocentron originated in the Chortis block (Fig. 6) in the late Eocene (36.7 Mya). From this block, ancestors of the first clade dispersed northward during the late Oligocene (25.9 Mya) with subsequent vicariance of *C. rafamoralesi* **sp. nov.** (currently in the Chortis block) and *C. yavapai* (currently in the Nearctic) in the middle Miocene (15.2 Mya). The ancestors of the second clade remained in the Chortis block, and started to radiate in the middle Miocene (12.3 Mya) with dispersal to north (to Mexican transition zone) and south (to South America). The clade with ancestors in Chortis block and Mexican transition zone had a subsequent cladogenesis between *C. ideolus* (currently in the Mexican transition zone) and *C. trilineatum* (currently in the Chortis and Maya blocks) in the late Miocene (7.9 Mya), whose process was indistinguishable between vicariance and dispersion. The clade with ancestors in the Chortis block (*C. carlosdelarosai* **sp. nov.** + *C. lausus*) and the clade with ancestors in South America and

Chorotega block diverged in the late Miocene (9.9 Mya), but the results could not distinguish the biogeographical event for this node either. Finally, the last clade diversified in Chorotega block and South America, with *C. pallas* (currently in South America) diverging in the first cladogenesis (8.5 Mya) and *C. immaculatum* (currently in South America) and *C. galesus* (currently in the Chorotega block) diverging in the second cladogenesis (7.6 Mya).

TAXONOMY

Under the evidence of polyphyly of the genus *Cnodocentron* sensu Schmid 1982, the subgenus *Caenocentron* is here elevated to generic status, and the genus *Cnodocentron* is now restricted to the Oriental species only. Here, we also present the revision *Caenocentron* **stat. nov.** describe new species and present an identification key.

GENUS *CNODOCENTRON* SCHMID, 1982

Cnodocentron Schmid, 1982:36 [Type species: *Cnodocentron girika* Schmid, 1982, original designation].

Cnodocentron was recovered as monophyletic based on the synapomorphies: female segment VIII with thickened setae (1:1); coxopodite margin produced posterad (31:1); sternum IX apical margin with projections or spines (12:1); harpago with subapical setal brush (44:2); setal brushes with elongate setae (45:1).

Diagnosis: forewing apex acute; hindwing transverse vein *r1-sr* present or absent; mesoscutelum edges straight; sternum V reticulated plate absent. Male genitalia: sternum IX apical margin with group of stout spines or elongated projections; preanal appendage mostly straight; coxopodite apical margin produced, projection narrow; harpago with brush of seta.

GENUS *CAENOCENTRON* (SCHMID, 1982) STAT. NOV.

Cnodocentron (*Caenocentron*) Schmid, 1982:42 [Type species: *Cnodocentron* (*Caenocentron*) *pallas* Schmid, 1982, original designation, as a subgenus].

Caenocentron stat. nov. was recovered as monophyletic based on the synapomorphies: coxopodite basoventral margin produced (28:1); coxopodite apical margin produced posterad (31:1); harpago basal stout spine present (38:1); basal plate apodeme apex directed ventrad (27:1); and coxopodite basomesal setae elongated (34:1).

Diagnosis: forewing apex rounded to subacute; hindwing transverse vein *r1-sr* present; mesoscutelum edges rounded; sternum V reticulated plate present. Male genitalia: sternum IX dorsal margin usually produced; preanal appendage usually thin and sigmoid; basal plate apodeme usually short and directed ventrad; coxopodite apical margin produced, projection narrow or broad; coxopodite ventral margin produced, ventral projection bearing brush of bristle-like setae; harpago basal third with a stout spine.

IDENTIFICATION KEY TO ADULT MALE OF *CAENOCENTRON* STAT. NOV.

1 Sternum IX apical margin produced in elongate processes (Figs 13B, 14A)... 2

1' Sternum IX apical margin not produced, concave (Fig. 8A, 8C)... 3

2(1) Sternum IX apical margin projection as two narrow, elongate processes (Fig. 13D)... ***C. rafamoralesi* sp. nov.**

2(1)' Sternum IX apical margin projection as broad, deltoid plate, with two short apical processes (Fig. 14C)... ***C. yavapai***

3(2) Coxopodite apical margin projection narrow, acute (Figs 16A, 20B)... 4

3(2)' Coxopodite apical margin projection broad (Figs 17A, 18A, 19B)... 5

4(3) Sternum IX, in lateral view, with apex truncate; coxopodite, in ventral view, with ventral projection having long and dense setae covering most of inner margin, including mesally; each coxopodite with inner face having one subapical short spine (Fig. 20B, 20D)... ***C. trilineatum***

4(3)' Sternum IX, in lateral view, with apex deltoid; coxopodite, in ventral view, with ventral projection having lateral setal brushes, mesally without setae; each coxopodite with inner face having two short spines (Fig. 16A, 16B)... ***C. ideolus***

5(3) Coxopodite apical margin with a short spine (Figs 17A, 18A)... 6

5(3)' Coxopodite apical margin without spine (Figs 15A, 19B)... 8

6(1) Coxopodite, in ventral view, inner margin with brush of long setae and a pair of long sublateral stout spines; harpago basal third strongly enlarged (Fig. 17A)... ***C. imaculatum***

6(1)' Coxopodite, in ventral view, inner margin with brush of long setae, without any long stout spines; harpago basal third slightly enlarged or not enlarged (Fig. 18A)... 7

7(6) Harpago base with a linear setal brush; coxopodite apical margin projection very broad until the apex, bearing a short spine on ventroapical margin (Fig. 18A)... ***C. lausus***

7(6)' Harpago base without any setal brush; coxopodite apical margin projection tapering to a rounded apex, bearing a short spine subapically (Fig. 8A)... ***C. carlosdelarosai*** **sp.nov.**

8(6) Inferior appendage presenting a lobe covered with brush of setae near harpago base; coxopodite median region with almost indiscernible small setules; paraproct dorsal margin without process, ventroapical margin rounded (Fig. 19B, 19C)... ***C. pallas***

8(6)' Inferior appendage without any brush of setae near harpago base; coxopodite median region with a transverse patch of setae; paraproct dorsal margin with short acute process, ventroapical margin acute (Fig. 15A)... ***C. galesus***

CAENOCENTRON CARLOSDELAROSAI SP. NOV.

(Figs 7A–B, 8A–C, 9A–D)

Diagnosis: Caenocentron carlosdelarosai **sp. nov.** can be diagnosed by the combination of the following characters: absence of stout spines on the ventral projection of coxopodite; shorter coxopodite in ventral view; the apical lobe of coxopodite narrow and with rounded margins; and the apical margin of sternum IX truncate in lateral view.

Adult (Fig. 7A–B): Forewing length 2.7–3.1 mm (n=3♂). Color (in alcohol) uniformly dark brown. Maxillary palp formula (I=II=III)-IV-V; segment IV shorter than sum of segments I-II-III; tibial spurs 2-4-3 in males and 2-4-4 in females, male hindleg apical spur unmodified. Venation: forewing fork II and IV present, 3 anal veins present; hindwing fork II and V present, transverse vein between R1 and SR present. Abdominal sternum V with anterolateral oval region with cuticle modified and reticulate.

Male genitalia (Fig. 8A–C): Tergum IX, in lateral view, narrow, height greater than length; in dorsal view, membranous mesally. Sternum IX, in lateral view, subquadrate, height greater than length; anterior margin truncate, with narrow and elongate apodeme; apical margin truncate; dorsal margin prominent; in ventral view, apical margin concave. Segment X membranous, fused to paraproct. Paraproct, in lateral view, oblong, dorsal margin sclerotized, with subapical short process; in dorsal view, middorsal margin sclerotized, not fused, meeting at mid length. Preanal appendage, in lateral view, strongly sinuous, slender, base and apex enlarged. Inferior appendage with coxopodite and harpago distinct. Coxopodite, in lateral view, with median region with setal brush; apical margin produced rounded, with subapical stout spine; basal surface with long ventral projection, which has a row of setae mesally and along its margin, apical setae longer; in ventral view, ventral projection with very long lateral setae and shorter mesal setae. Harpago, in lateral view, slender, basal third with short spine; in dorsal view, basal third slightly enlarged. Basal plate, in lateral view, directed ventrad; in ventral view, short. Phallus tubular, very long and slender, base flared, reaching segment V; apex slightly enlarged.

Female genitalia (Fig. 9A–D): Telescopically elongate, forming slender oviscapt. Segment VIII synscleritous, dorsally open, membranous, posterior margin with linear row of long setae; each anterolateral margin with narrow, very elongate apodeme extending anteriorly until segment VI. Intersegmental membrane VIII–IX well developed. Segment IX tubular, slender, covered with annulated striations; longer than segment VIII, open ventrally; each anterolateral margin with narrow, very elongate apodeme extending anteriorly to segment V. Gonopod VIII elongate until segment X, semi-membranous; in lateral view, tapered apically; in ventral view, apex truncate,

bearing line of subapical setae. Gonopod IX, rim-like, narrow, elongate. Segment X small, covered with sensilla. Cercus narrow, digitiform.

Etymology: Caenocentron carlosdelarosai is named in honor of Dr. Carlos Luis de la Rosa in recognition of his decades of research on the Chironomidae of Costa Rica.

Distribution: Costa Rica

Material examined. Type material: Holotype. COSTA RICA, Guanacaste, Area de Conservacion Guanacaste, Sector San Cristobal, Estacion San Geraldo, 10° 52' 48" N, 85° 23' 20.4" W; 575m asl, 16.xii.2013, Malaise trap, D.H. Janzen & W. Hallwachs leg., (♂ in alcohol, BIOUG23036-H02) – Paratypes. same data as holotype except: 21.x.2013 (♂ BIOUG20201-D06); 18.xi.2013 (♂ MZSP); 23.xii.2013 (♂ BIOUG28070-A05); 26.vii.2013 (♀ MZSP); 27.i.2014 (♀ BIOUG23963-A07); 23.ix.2013 (♀ BIOUG19826-E05); 21.viii.2013 (♀ BIOUG20201-D02); 21.viii.2013 (♀ BIOUG20201-D03). 26.viii.2013, Malaise trap (♀ pinned BIOUG19587-H05).

Remarks: The COI sequences of *C. carlosdelarosai* **sp. nov.** formed two clusters, the male paratypes from each cluster did not present any significant difference in the male genitalia (Fig. 12). The genetic distance between each cluster was 3.8%, with a mean intraspecific distance of 2%. The genetic distance between *C. carlosdelarosai* **sp. nov.** and *C. rafamoralesi* **sp. nov.** was 10%; and between *C. trilineatum* was 8.1%. The overall mean genetic distance between all included xiphocentronids was of 15.0%.

Currently, *C carlosdelarosai* **sp. nov.** is the only known female in the clade which males have coxopodite with longer setal-brushes. In comparison with the females of the clade with *C. yavapai* and *C. rafamoralesi* **sp. nov.**, the female of *C. carlosdelarosai* has the gonopod VIII conspicuous at the sides of the segment IX, while in *C. yavapai* and *C. rafamoralesi* **sp. nov.** the gonopod VIII is completely fused with the segment IX and seen just as a narrow apodeme-like structure. Also, *C. yavapai* and *C. rafamoralesi* **sp. nov.** have a pair of inner sclerites (gonopod IX) at the apex of the genitalia, but in *C. carlosdelarosai* **sp. nov.** they are not visible.

CAENOCENTRON RAFAMORALESI SP. NOV.

(Figs 13A–D, 10A–D)

Diagnosis: Caenocentron rafamoralesi sp. nov. is similar to *C. yavapai* by presenting an elongate projection on the apical margin of sternum IX. It can be diagnosed by these projections on sternum IX forming a pair of elongate and narrow processes; by the acute spine-like apical projection of coxopodite; and by having the ventral projections of coxopodite short and not fused with each other.

Adult (Fig. 13A): Forewing length 4.0–4.3 mm (n=2♂). Color (in alcohol) uniformly dark brown. Maxillary palp formula (I=II=III)-IV-V; segment IV shorter than sum of segments I-II-III; tibial spurs 2-4-3 in males and 2-4-4 in females, male hindleg apical spur unmodified. Venation: forewing fork II and IV present, 3 anal veins present; hindwing fork II and V present, transverse vein between R1 and SR present. Abdominal sternum V with anterolateral oval region with cuticle modified and reticulate.

Male genitalia (Fig. 13B–D): Tergum IX, in lateral view, narrow, height greater than length; in dorsal view, short. Sternum IX, in lateral view, rounded, about as long as high; anterior margin deltoid, tapering to narrow apodeme; apical margin with elongate process; dorsal margin slightly prominent; in ventral view, apical margin with two elongate medial processes, as long as sternum length. Segment X membranous, fused to paraproct. Paraproct, in lateral view, oblong, setose, dorsal margin, sclerotized, without any process, ventroapically subacute; in dorsal view, middorsal margins distinctly sclerotized subapically, fused, with rows of setae mesally and laterally. Preanal appendage, in lateral view, slightly sinuous, enlarged subapically, tapered apically. Inferior appendage with coxopodite and harpago fused, dorsally with wide gap between the articles. Coxopodite, in lateral view, apical margin with narrow and acute projection; basomesal surface with short projection covered with brush of short setae; in ventral view, basomesal surface of each coxopodite not fused mesally, covered with short setae. Harpago, in lateral view, slender, basal third with short basal spine, many sparse spines present until midlength; in dorsal view, basally enlarged. Basal plate, in lateral view, directed anterad; in ventral view, elongate, acute. Phallus tubular, very long and slender, base flared, reaching segment V; apex slightly enlarged.

Female genitalia (Fig. 10A–D): Telescopically elongate, forming slender oviscapt. Segment VIII synscleritous, dorsally open, membranous, posterior margin with linear row of long setae; each anterolateral margin with narrow, very elongate apodeme extending anteriorly until segment VI. Intersegmental membrane VIII–IX well developed. Segment IX tubular, slender, covered with annulated striations; longer than segment VIII; each anterolateral margin with narrow, very elongate apodeme extending anteriorly to segment V. Gonopod VIII elongate until segment IX; in lateral view, appearing as narrow, sclerotized rim along IX segment; in ventral view, apex semi-membranous. Gonopod IX rod-like, sclerotized. Segment X small, covered with sensilla. Cercus narrow, digitiform.

Remarks: The COI sequences of *C. rafamoralesi* **sp. nov.** had a mean intraspecific genetic distance of 1%. The genetic distance between *C. rafamoralesi* **sp. nov.** and *C. carlosdelarosai* **sp. nov.** was of 10%; and between *C. trilineatum* was 9.6%.

Etymology: Caenocentron rafamoralesi is named in honor of stream parataxonomist Rafael Angel Morales Cueto in recognition of his 30 years of research and station management for Estación Biológica Maritza in Sector Orosí of Área de Conservación Guanacaste, Costa Rica.

Distribution: Costa Rica

Material examined. Type material: Holotype. COSTA RICA, Guanacaste, Area de Conservacion Guanacaste, Sector Cacao, Derrumbe, 10° 55' 45.12" N, 85° 27' 51.48" W; 1220m asl, 30.iv.2015, Malaise trap, DH Janzen, W Hallwachs leg., (♂ in alcohol BIOUG36194-F08). – Paratypes. same data as holotype except: 23.iv.2015 (♂ in alcohol BIOUG33413-E09); and 30.x.2014 (♀ in alcohol BIOUG31506-F08).

CAENOCENTRON YAVAPAI MOULTON & STEWART, 1997

(Figs 11A–C, 14A–C)

Cnodocentron (*Caenocentron*) *yavapai* Moulton & Stewart, 1997: 347, [Type locality: United States of America, Arizona: Yavapai Co., Bubbling Springs, Coconino

National Forest, USNM; ♂, larva, pupa]. – Blinn & Ruiter 2005: 71 [emergence, community structure, distribution]. – Ruiter 2006:528 [♀].

Diagnosis: Caenocentron yavapai is similar to *C. rafamoralesi* **sp. nov.** by the apical projection of sternum IX. It is distinguished by the trifid apical projection of coxopodite; dorsal margin of sternum IX not prominent, and the broad elongated apex of sternum IX with a pair of short processes.

Adult: Forewing length 4.0 mm (n=2♂). Color (in alcohol) uniformly dark brown. Maxillary palp formula (I-II-III)-IV-V; segment IV shorter than sum of segments I-II-III; tibial spurs 2-4-3 in males, 2-4-4 in females, male hindleg apical spur unmodified. Venation: forewing fork II and IV present, 3 anal veins present; hindwing fork II and V present, transverse vein between R1 and SR present. Abdominal sternum V with anterolateral oval region with cuticle modified and reticulate.

Male genitalia (Fig. 14A–C). Tergum IX, in lateral view, narrow, height greater than length, bearing finger-like lobe with spines, lobe placed between tergum IX, paraproct and preanal appendage. Sternum IX in lateral view, subdeltoid, longer than higher, anterior margin deltoid, with narrow apodeme, apical margin produced, acute, dorsal margin not prominent; in ventral view apical margin produced, deltoid, with two apical points. Preanal appendage long, sinuous, narrowed subbasally, enlarged at base and apically. Tergum X membranous, fused to paraproct. Paraproct, in lateral view, trapezoidal, dorsal margin with spinelike-setae, laterally sclerotized with subapical spine, apex subacute; in dorsal view, mesally sclerotized, fused, with pair of subapical spinelike-setae. Inferior appendage coxopodite and hapago distinct. Coxopodite median region with lobe tipped with setae; apical margin produced, trifid with each process with stout spine at apex, middle process longest, with subapical spine, ventral process shortest; basal surface with brush of setae, without projection; in ventral view, basal surface with setae of same length. Basal plate, in lateral view, directed ventrad; in ventral view, long, acute. Harpago in lateral view, slender, slightly enlarged basally, subbasally with short spine and small setules. Phallus tubular, very long and slender, base flared, reaching segment V; apex slightly enlarged.

Female genitalia (Fig. 11A–C): Telescopically elongate, forming slender oviscapt. Segment VIII synscleritous, dorsally open, membranous, posterior margin with linear row of long setae; each anterolateral margin with narrow, very elongate apodeme extending anteriorly until segment VI. Intersegmental membrane VIII–IX well developed. Segment IX tubular, slender, covered with annulated striations; longer than segment VIII; each anterolateral margin with narrow, very elongate apodeme extending anteriorly to segment V. Gonopod VIII elongate until segment IX; in lateral view, appearing as narrow, sclerotized rim along IX segment; in ventral view, apex semi-membranous. Gonopod IX as pair of mesal sclerotized, elongate rod-like structures. Segment X small, covered with sensilla. Cercus narrow, digitiform.

Distribution: Southwest of the United States.

Material examined. Type material: Paratype: UNITED STATES. Arizona, Yavapai Co.: Bubbling Springs, Coconino National Forest, off Forest Service Rd. 134, approximately 1.5 km N Page Springs (town), 22.iv.1993, 6 m, malaise trap S.R. Moulton and K.W. Stewart leg., (2♂ in alcohol, UMSP000021747).

CAENOCENTRON GALESUS SCHMID, 1982

(Fig. 15A–B)

Cnodocentron (*Caenocentron*) *galesus* Schmid, 1982: 44 [Type locality: Costa Rica, 2.8 mi E. of Golfito; USNM; ♂]. – Holzenthal, 1988: 58 [distribution]. – Aguila 1992: 537 [distribution]. – Armitage *et al.* 2015: 5 [checklist]. – Armitage & Cornejo 2015: 193. [checklist]. – Holzenthal & Calor 2017: 454 [catalog].

Diagnosis: Cnodocentron galesus is similar to *C. immaculatum* and *C. pallas* by presenting a pair of stout spines on the ventral projection of coxopodite. C. *galesus* can be diagnosed by the truncate apical margin of sternum IX in lateral view; and the median region of coxopodite with a transverse patch of setae.

Adult: Forewing length 2.7 mm (n=1♂). Color (pinned) dark with three short white vertical bars: near the basal third of wing, at the end of cubital vein, and at pterostigma.

Maxillary palp formula (I-II-III)-IV-V; segment IV shorter than sum of segments I-II-III; male tibial spurs 2-4-3, male hindleg apical spur unmodified. Venation: forewing fork II and IV present, 3 anal veins present; hindwing fork II and V present, transverse vein between R1 and SR present. Abdominal sternum V with anterolateral oval region with cuticle modified and reticulate.

Male genitalia (Figs 15A–B): Tergum IX, in lateral view, narrow, height greater than length. Sternum IX, in lateral view, subquadrate, height greater than length, anterior margin truncate, with narrow and elongate apodeme, apical margin truncate, dorsal margin prominent; in ventral view, apical margin concave. Segment X membranous, fused to paraproct. Paraproct, in lateral view, trapezoidal, dorsal margin, sclerotized, with short process, ventroapically acute. Preanal appendage, in lateral view, strongly sinuous, slender, apex enlarged. Inferior appendage, coxopodite and harpago distinct. Coxopodite, in lateral view, median region with transverse patch of setae; apical margin produced, rounded; basal surface with long ventral projection. Ventral projection with stout spine and rows of setae mesally and along its margin, apical setae longer; in ventral view, ventral projection lateral setae very long, mesal setae short, with pair of strong lateral spines. Harpago, in lateral view, slender, elongate, basal third with short spine; in dorsal view, basal third with two weak thickenings. Basal plate, in lateral view, directed ventrad. Phallus tubular, very long and slender, base flared, reaching segment V; apex slightly.

Distribution: Costa Rica, Panama.

Material examined. Type Material: Holotype male. COSTA RICA, Puntaneras, 2.8 mi E. of Golfito 3-4.vii.1967, O. S. Flint & B. Ortiz leg., (♂ pinned, USNMENT1028602).

CAENOCENTRON IDEOLUS SCHMID, 1982

(Fig. 16A–B)

Cnodocentron (*Caenocentron*) *ideolus* Schmid, 1982: 106 [Type locality: Mexico, Lomas de Chapultepec, D.F.; INHS; ♂]. – Holzenthal & Calor 2017: 454 [catalog].

Diagnosis: Caenocentron ideolus is similar to *C. trilineatum* by the narrow apical projection of coxopodite. It can be diagnosed by the presence of an elongate ventral process on the paraproct; coxopodite with the ventral projection of coxopodite short and with shorter setae; harpago with a basal brush of setae; and sternum IX overall deltoid in lateral view.

Adult: Forewing length 3.0 mm.

Male genitalia (Fig. 16A–B): Tergum IX, in lateral view, narrow, height greater than length. Sternum IX in lateral view, deltoid, about as high as long, anterior margin truncate, with narrow and elongate apodeme, apical margin acute, dorsal margin prominent; in ventral view apical margin straight with a medial concavity. Preanal appendage, in lateral view, strongly sinuous, slender, apex enlarged. Segment X membranous, fused to paraproct. Paraproct, in lateral view, oblong, dorsal margin with short process, laterally sclerotized, ventroapically subacute, lined with strong setae, ventrally with strong elongate process. Inferior appendage coxopodite and hapago distinct. Coxopodite, in lateral view, apical margin produced, narrow, subacute, with subapical spine; mesoventral margin with long spine; basal surface with short ventral projection. Ventral projection with rows of setae; in ventral view, inner surface with two spines in mesoventral and subapical position, presenting small lobe with setae near mesoventral spine. Ventral projection with lateral setae short, withouth mesal setae. Harpago, in lateral view, slender, basal third enlarged, with short spine and basal setal brush. Basal plate, in lateral view, directed ventrad; in ventral view, short.

Distribution: Mexico.

Material examined: None (synopsis based on Schmid, 1982).

CAENOCENTRON IMMACULATUM FLINT, 1991

(Fig. 17A–C)

Cnodocentron (*Caenocentron*) *immaculatum* Flint, 1991: 34 [Type locality: Colombia, Dpto. Antioquia, Quebrada la Jimenez, Sopetran; USNM; ♂]. – Muñoz-Quesada, 2000: 281 [checklist]. – Holzenthal & Calor, 2017: 454 [catalog].

Diagnosis: Cnodocentron immaculatum is similar to *C. galesus* and *C. pallas* by presenting a pair of stout spines on the ventral projection of coxopodite. It can be differentiated by the greatly enlarged base of harpago bearing a brush of setae.

Adult: Forewing length 3.0 mm (n=1♂). Color (in alcohol) uniformly dark brown. Maxillary palp formula (I-II-III)-IV-V; segment IV shorter than sum of segments I-II-III; male tibial spurs 2-4-3, male hindleg apical spur unmodified. Venation: forewing fork II and IV present, 3 anal veins present; hindwing fork II and V present, transverse vein between R1 and SR present. Abdominal sternum V with anterolateral oval region with cuticle modified and reticulate.

Male genitalia (Fig. 17A–C): Tergum, IX in lateral view, narrow, height greater than length. Sternum IX, in lateral view, deltoid, about as high as long, anterior margin truncate, with narrow, elongate apodeme, apical margin rounded, dorsal margin prominent; in ventral view, apical margin concave. Segment X membranous, fused to paraproct. Paraproct, in lateral view, trapezoidal, dorsal margin with short process, ventroapically subacute; in dorsal view, middorsal margins sclerotized, not fused. Preanal appendage, in lateral view, strongly sinuous, slender, slightly enlarged apically. Inferior appendage coxopodite and hapago distinct. Coxopodite, in lateral view, median region with very short setae; apical margin produced, broad, apex truncate and bearing stout spine near ventral margin; basal surface with ventral projection. Ventral projection with stout spine and rows of setae mesally and along its margin, apical setae longer; in ventral view, ventral projection with long lateral setae, short mesal setae, and two stout sublateral spines. Harpago, in lateral view, slender, basal third strongly enlarged, bearing short spine and basal setal brush. Basal plate, in lateral view, directed ventrad; in ventral view short. Phallus tubular, very long and slender, base flared, reaching segment V; apex slightly enlarged.

Distribution. Colombia.

Material examined. Type material: Holotype. COLOMBIA: Antioquia: Quebrada La Jimenez, Mun. Sopetran. 7.ii.1984, U. Matthias leg., (♂ in alcohol, USNM).

CAENOCENTRON LAUSUS SCHMID, 1982

(Fig. 18A–B)

Cnodocentron (*Caenocentron*) *lausus,* Schmid, 1982: 44 [Type locality: Nicaragua, 4.2mi W of Villa Somoza; USNM; ♂]. – Maes & Flint, 1988: 3 [distribution]. – Maes, 1999: 1188 [checklist]. – Chamorro-Lacayo *et al.*, 2007: 47 [checklist]. – Holzenthal & Calor, 2017: 454 [catalog].

Diagnosis: Caenocentron lausus can be differentiated from its congeners by presenting the conjucntion of the following characters: coxopodite with broad apical projection bearing an apicoventral point; ventral projection without a pair of stout spines; and harpago basal third enlarged and with a linear setal brush.

Adult: Forewing length 2.5 mm (n=1♂). Color (pinned) dark with three short white vertical bars: near the basal third of wing, at the end of cubital vein, and at pterostigma. Maxillary palp formula (I-II-III)-IV-V; segment IV shorter than sum of segments I-II-III; male tibial spurs 2-4-3, male hindleg apical spur unmodified. Venation: forewing fork II and IV present, 3 anal veins present; hindwing fork II and V present, transverse vein between R1 and SR present. Abdominal sternum V with anterolateral oval region with cuticle modified and reticulate.

Male genitalia: (Fig. 18A–B) Tergum IX, in lateral view narrow, height greater than length. Sternum IX, in lateral view, subquadrate, about as high as long, anterior margin truncate, with narrow and elongate apodeme, apical margin subtruncate, dorsal margin prominent; in ventral view, apical margin concave. Segment X membranous, fused to paraproct. Paraproct in lateral view, trapezoidal, dorsal margin sclerotized, with subapical short process ventroapically acute. Preanal appendage, in lateral view, strongly sinuous, slender, slightly enlarged apically. Inferior appendage coxopodite and hapago distinct. Coxopodite, in lateral view, median region with rugose area; apical margin produced oblong, subtruncate, with small ventroapical spine; basal surface with ventral projection. Ventral projection with rows of setae mesally and along its margin, apical setae longer; in ventral view ventral projection with lateral setae longer, mesal setae shorter. Harpago, in lateral view, slender, basal third enlarged, bearing short spine

and linear basal setal brush. Basal plate, in lateral view, directed ventrad; in ventral view short. Phallus tubular, very long and slender, base flared, reaching segment V; apex slightly enlarged.

Distribution: Nicaragua.

Material examined. Type Material: Holotype. NICARAGUA: Chontales: 4.2 mi. W. of Villa Somoza, 29.vii.1967, O.S. Flint leg., (♂ pinned, USNMENT01028603).

CAENOCENTRON PALLAS SCHMID, 1982

(Fig. 19A–D)

Cnodocentron (*Caenocentron*) *pallas* Schmid, 1982: 44 [Type locality: Panama, Canal Zone, Gamboa, Rio Agua Salud; USNM; ♂]. – Aguila, 1992: 537 [distribution]. – Armitage *et al.*, 2015: 5 [checklist]. – Armitage & Cornejo, 2015: 193 [checklist]. – Holzenthal & Calor, 2017: 454 [catalog].

Diagnosis: Cnodocentron pallas present a pair of stout spines on the ventral projection of coxopodite as in *C. galesus* and *C. immaculatum*. It can be diagnosed by presenting on the dorsal margin of coxopodite a mesal process covered with brush of setae; and by the rounded apical projection of coxopodite without spine.

Adult: Forewing length 2.75 mm (n=1♂). Color (pinned) dark with three short white vertical bars: near the basal third of wing, at the end of cubital vein, and at pterostigma. Maxillary palp formula (I-II-III)-IV-V; segment IV shorter than sum of segments I-II-III; male tibial spurs 2-4-3, male hindleg apical spur unmodified. Venation (Fig. 19A): forewing fork II and IV present, 3 anal veins present; hindwing fork II and V present, transverse vein between R1 and SR present. Abdominal sternum V with anterolateral oval region with cuticle modified and reticulate.

Male genitalia (Fig. 19B–D): Tergum IX, in lateral view, narrow, height greater than length. Sternum IX, in lateral view, subquadrate, about as high as long, anterior margin truncate, with narrow and elongate apodeme, apical margin truncate, dorsal margin prominent; in ventral view apical margin concave. Segment X membranous, fused to

paraproct. Paraproct, in lateral view, trapezoidal, dorsal margin sclerotized, without process; laterally sclerotized with spine-like setae, ventroapically rounded; in dorsal view, not fused, middorsal margins not fused, meeting subapically. Preanal appendage, in lateral view, strongly sinuous, slender, enlarged apically. Inferior appendage coxopodite and harpago distinct. Coxopodite, in lateral view, with dorsal lobe covered by setae, median region with small setules; apical margin produced, broad, rounded; basal surface with ventral projection. Ventral projection with stout spine and rows of setae mesally and along its margin, apical setae longer; in ventral view, ventral projection with lateral setae longer, mesal setae shorter, and two strong lateral spines. Harpago, in lateral view, basal third slightly enlarged, bearing subbasal short spine and lobe with setal brush appearing derived from coxopodite. Basal plate, in lateral view, directed ventrad; in ventral view short. Phallus tubular, very long and slender, base flared, reaching segment V; apex slightly enlarged.

Distribution: Panama.

Material examined. Type material: Holotype: PANAMA: Canal Zone: Gamboa, Río Agua Salud, 9°7'14.8794", -79°42'56.88", vii.1967, Wirth, W. W. leg., (♂ pinned, USNMENT1028604).

CAENOCENTRON TRILINEATUM (MOSELY, 1934)

(Fig. 20A–F)

Melanotrichia trilineata Mosely, 1934: 140 [Type locality: Mexico, Teapa, Tabasco; BMNH; ♂]. – Fischer, 1962: 234 [distribution].

Xiphocentron trilineatum – Bueno-Soria & Flint, 1978: 197 [distribution].

Caenocentron (*Caenocentron*) *trilineatum* – Schmid, 1982: 112 [checklist]. – Holzenthal & Calor, 2017:454 [catalog].

Diagnosis: Caenocentron trilineatum is similar to *C. ideolus* by the narrow apical projection of coxopodite. It can be differentiated by the median region of coxopodite presenting two small lobular mesal processes; and paraproct with distinct lateral sclerotized ridge bearing spine-like setae.

Adult: Forewing length 3.0 mm (n=1♂). Color (pinned) dark with three short white vertical bars: near the basal third of wing, at the end of cubital vein, and at pterostigma. Maxillary palp formula (I-II-III)-IV-V; segment IV shorter than sum of segments I-II-III; male tibial spurs 2-4-3, male hindleg apical spur unmodified. Venation (Fig. 20A): forewing fork II and IV present, 3 anal veins present; hindwing fork II and V present, transverse vein between R1 and SR present. Abdominal sternum V with anterolateral oval region with cuticle modified and reticulate.

Male genitalia: (Fig. 20B–F) Tergum IX, in lateral view, narrow, height greater than length. Sternum IX, in lateral view, subquadrate, about as high as long, anterior margin truncate, with narrow and elongate apodeme, apical margin truncate, dorsal margin prominent; in ventral view, apical margin concave. Tergum X membranous, fused to paraproct. Paraproct in lateral view, trapezoidal, dorsal margin with acute process, laterally with distinct sclerotized ridge bearing spine-like setae, ventroapically acute, with subapical spines; in dorsal view, middorsal margins sclerotized, not fused, meeting at mid length. Preanal appendage long, slender, evenly sinuated in lateral aspect, apex slightly enlarged. Inferior appendage coxopodite and hapago distinct. Coxopodite, in lateral view, apical margin produced, narrow, acute, with subapical spine; median region with sparse short setae, and two lobular mesal processes covered with setae, one lobe very smaller than other, basal surface with ventral projection. Ventral projection with row of setae mesally and along its margin, apical setae longer; in ventral view, covered with brushes of setae, sublateral and mesal setae distinctly thicker, sublateral setae longer. Harpago long, slender, base slightly enlarged, bearing subbasal spine and small setules. Phallus tubular, very long and slender, base flared, reaching segment V; apex slightly enlarged.

Distribution: El Salvador; Guatemala; Mexico.

Material examined: EL SALVADOR: Los Chorros: nr. Santa Tecia, 5.vii.1966. Flint & Ortiz leg., (♂ pinned, USNM).

DISCUSSION

The phylogeny indicated that *Cnodocentron* sensu Schmid (1982) is polyphyletic with the species from Asia forming a clade together with *Melanotrichia,* and the species from New Word forming another clade together with species of *Xiphocentron*. Our data also revealed that the cladogenesis between these two clades occurred during the Paleocene-Eocene Thermal Maximum around 56 Mya (Fig. 6). This divergence dating corroborates Schmid's (1982) hypothesis of the xiphocentronid groups dispersing through Asia and America during the warm periods of the Eocene. This period fits the time when both the Beringia and the Thulean routes via Greenland were available (Brikiatis, 2014). However, the current absence of xiphocentronids in Europe and northern Africa, suggest a reduced possibility for the use of the Thulean route. During the early Eocene, the climate was much warmer than today, with subtropical rainforests occurring in high latitudes; at the end of the Eocene, the climate became cooler, and most dispersals of frost-intolerant groups through Beringia stopped (Tiffney, 1985; Sanmartín *et al.*, 2001). This warmer period allowed thermophilic species of plants and animals to cross the Bering land bridge connecting America and Asia (Sanmartín *et al.*, 2001; Brunke *et al.*, 2017). Possibly the xiphocentronids were widespread through these Boreotropic forests during the early Eocene. With the climate cooling down at the end of the Eocene, the xiphocentronids retreated their distributions mainly to the current tropical zone. In the case of genera studied here, *Cnodocentron* diversified in southern parts of East Palearctic, while *Caenocentron* in southern USA, Mesoamerica, and north of South America. Although *Cnodocentron* and *Caenocentron* have distinct evolutionary histories, both genera evolved in regions with strong geological activity.

The dispersal of the *Cnodocentron* ancestors to the Indian plate around 41 Mya coincides with a period of increasing species interchange between India and Asia mainland when the two regions were probably completely connected (Klaus *et al.*, 2016) (Fig. 21A). The divergence between the *Cnodocentron* clades in Southeast Asia and Himalaya (Indian plate edge) occurred during the Oligocene (around 30 Mya). This period is concomitant with a significant uplift of the Sino-Burmese and Annamite mountain ranges, as well as the Natuna Arch, and West Sarawak uplands, which formed a dispersal route for temperate species from Indochina to Borneo, with the occurrence of Laurasian conifers and temperate plants as *Pinus*, *Alnus* and *Lithocarpus* (Morley 2018). This cladogenesis is indicated in the biogeographical analysis as a dispersal

event, which isolated the *Cnodocentron* populations in the Himalaya foothills. During the Middle Miocene climatic optimum (17–14 Mya), the Himalaya uplift intensified resulting in increased temperature and orographic rainfall in northern India (Ding *et al.*, 2017; Morley, 2018). A rain forest belt connecting the lower Himalaya and the Southeast Asia highlands was formed, which resulted in the central peak of biotic interchange between the Indian subcontinent and Asia mainland (Songtham *et al.*, 2003; Klaus *et al.*, 2016). This biotic interchange was reduced after 14 Mya (Klaus *et al.*, 2016). This period is marked by seasonally drier conditions, which intensified during the late Miocene with successive cooler and drier global climates (Zachos *et al.*, 2001), resulting in the expansion of the grasslands and the establishment of arid climates in northern India (Quade *et al.*, 1989; Guleria, 1992). These events were probably related to the expansion of the clade (*C. brogimarus* (*C. tchaturbhuja* + *C. filamenta*) around 15 Mya with the formation of the rainforest belt, and the subsequent vicariant event between *C. tchaturbhuja* and *C. filamenta* around 9 Mya (Fig. 21A), which was coincident with the drought intensification when the vegetation from northern India changed from forest vegetation to grasslands (Srivastava *et al.*, 2018).

The biogeographical analysis indicates that the New Word *Caenocentron* probably originated in the Chortis block during the late Eocene (37 Mya) (Fig. 6). There are two competing models for the geologic evolution of the Chortis block: (1) in the traditional model, this tectonic block was placed adjacent to southwestern Mexico until the early Eocene (49 Mya) when it detached from Mexico and started moving southeastwards, taking its present position at the south of the Maya block in the early Miocene (22 Mya) (Schaff *et al.*, 1995; Mann, 2007; Silva-Romo *et al*., 2018); (2) in the Pacific model, the Chortis block at 45 Mya was placed in the Pacific ocean, southwestern of its present position (Keppie & Morán-Zenteno, 2005). The traditional model seems to fit better with our results, as the dispersal of xiphocentronids to the block in the late Eocene would be less probable in such a distant position (Fig. 21B).

Caenocentron diverged into a clade that remained in the Chortis block and another clade that dispersed to the north during a period of climate warming in the late Oligocene (25 Mya) (Guitián *et al.*, 2019). The clade that dispersed to the north subsequently diverged in *C. rafamoralesi* **sp. nov.** and *C. yavapai* during the climate cooling and drying after the Middle Miocene (Zachos *et al.*, 2001) (Fig. 21B).

Caenocentron rafamoralesi **sp. nov.** is known from areas nearby the Santa Elena peninsula, a primitive island arc geologically associated with the Chortis block and dated to the early Cretaceous (Hauff *et al.*, 2000). The long distributional gap between *C. rafamoralesi* **sp. nov.** and *C. yavapai* in the Nearctic may suggest the extinction or the existence of undescribed species related to this clade along the west coast of Mexico. The clade that remained in the Chortis block diverged around 12 Mya dispersing to the north and south. The ancestors of the clade that dispersed to the north reached the Mexican Transition Zone with a subsequent divergence between *C ideolus* and *C. trilineatum*, around 7.8 Mya. This cladogenetic event may be associated with the orogenic processes of the Trans Mexican Volcanic Belt in the Miocene and the intensification of silicic volcanism around 7.5 – 3 Mya (Mastretta-Yanes *et al.*, 2015).

The clade (*C. pallas* (*C gallesus* + *C. immaculatum*)), currently in Chorotega block and South America, diverged from the species in the Chortis block (*C. carlosdelarosai* **sp. nov.** and *C. lausus*) around 10 Mya. The collision between Central America and South America started around 24 Mya (Montes *et al.*, 2012). During most of this period, the Chorotega block was an island arc that then turned into a peninsula, with evidence of full connection to the Chortis block around 22 Mya (Kirby *et al.*, 2008). Although the complete closure of the Panama land bridge only occurred around 3 Mya (O'Dea, 2016), evidence indicates that much of the land was above sea level around 15-13 Mya (Montes *et al.*, 2015). A shallowing of the Central American seaway occurred from 12.8 to 9.5 Mya, and by 8.6 Mya most of the Darien region had emerged (Coates *et al.*, 2004; Leigh *et al.*, 2013). These geological events are in agreement with the *Caenocentron* dispersal to South America at 9.9 and 8.5 Mya. A rise in the sea-level, around 7–6 Mya (Coates *et al.*, 2004), could be related to the subsequent vicariant event between *C. immaculatum* and *C. gallesus,* although the statistical support for the relationship of these species is too weak to justify any conclusive statement.

CONCLUSION

This study provides the first phylogenetic hypotheses for *Cnodocentron* sensu Schmid (1982), which was recovered as polyphyletic, with each subgenera being more closely related to other genera from the same biogeographical region than to each other. Consequently, from the present study, each subgenus has generic status. The Schmid

(1982) hypothesis of divergence of Oriental and Neotropical clades during thermal events was corroborated, with the estimated mean age of the divergence closely associated with the Paleocene-Eocene Thermal Maximum event. The mean divergence time estimations using morphological and COI data were congruent with known geological and climatic events as: (1) the land connection between Indian Plate and Asia (~41 Mya); (2) the uplift of Indo-china mountain ranges (~30 Mya); (3) the formation of a tropical forest belt between the Himalayas and Southeast Asia (~15 Mya); (4) the increasing of aridity in Northern Mexico after the Middle Miocene (~15 Mya); (5) the intensification of volcanism in the Trans Mexican Volcanic Belt around 8 Mya; and (6) the increasing contact between the Central America and the South America around 10 Mya. Given the current known distribution and the available phylogenetic and paleontological data, we provide the first biogeographical hypothesis for *Caenocentron* and *Cnodocentron*. This hypothesis supports the origin of *Cnodocentron* associated with the dispersion of species to the Indian plate in its progressive collision with Asia; and the radiation of *Caenocentron* associated with the detachment and southward movements of the Chortis block, and the colonization of South America after 10 Mya. These results shed light on the diversification of these two genera and contribute to a better understanding of the diversification process of Xiphocentronidae.

REFERENCES

Aguila Y. 1992. Systematic catalogue of the caddisflies of Panama (Trichoptera). In: Quintero D, Aiello A (Eds) Insects of Panama and Mesoamerica: Selected Studies. Oxford University Press, Oxford, 532–548.

Armitage BJ, Cornejo A. 2015. Orden Trichoptera (Insecta) en Panamá: Listas de especies y su distribución por cuencas y unidades administrativas. *Puente Biológico* 7: 175–199.

Armitage BJ, Harris SC, Arefina-Armitage TI, Corne A. 2015. The Trichoptera of Panama. III. Updated species list for caddisflies (Insecta: Trichoptera) in the Republic of Panama. *Insecta Mundi* 0442: 1–16.

Banks N. 1941. New neuropteroid insects from the Antilles. *Memorias de la Sociedad Cubana de Historia Natural* 15: 385–402, plates 343–345.

Blahnik RJ, Holzenthal RW, Prather AL. 2007. The lactic acid method for clearing Trichoptera genitalia. In: Bueno-Soria, J., Barba-Álvarez, R., & Armitage, B. (Eds.), *Proceedings of the XIIth International Symposium on Trichoptera.* The Caddis Press, Columbus, Ohio, 9–14.

Blinn DW, Ruiter DE. 2005. Caddisfly (Trichoptera) community structure and distribution in Arizona, USA: effects of selected environmental determinants. In: Tanida K, Rossiter A (Eds) *Proceedings of the 11th International Symposium on Trichoptera.* Tokai University Press, Kanagawa, 63–71.

Brauer F. 1870. Ueber Xiphocentron. eine neue Hydropsychidengattung. Verhandlungen der Kaiserlich-königlichen. *Zoologischen-Botanischen Gesellschaft in Wien* 20: 66.

Brikiatis L. 2014. The De Geer, Thulean and Beringia routes: key concepts for understanding early Cenozoic biogeography. *Journal of Biogeography* 41: 1036–1054. https://doi.org/10.1111/jbi.12310

Brunke AJ, Chatzimanolis S, Metscher BD, Wolf-Schwenninger K, Solodovnikov A. 2017. Dispersal of thermophilic beetles across the intercontinental Arctic forest belt during the early Eocene. *Scientific Reports* 7(1): 12972. https://doi.org/10.1038/s41598-017-13207-4

Bueno-Soria J, Flint OS. 1978. Catálogo sistemático de los tricopteros de México (Insecta: Trichoptera), con algunos registros de Norte, Centro y Sudamérica. *Anales del Instituto de Biología, Universidad Nacional Autónoma de México, Serie Zoología* 49: 189–218.

Chamorro-Lacayo ML, Maes JM, Holzenthal RW, Blahnik RJ. 2007. Updated checklist of the Trichoptera of Nicaragua. In: Bueno-Soria J, Barba-Álvarez R, Armitage BJ (Eds) *Proceedings of the 12th International Symposium on Trichoptera.* The Caddis Press, Columbus, Ohio, 37–50.

Close RA, Friedman M, Lloyd GT, Benson RB. 2015. Evidence for a mid-Jurassic adaptive radiation in mammals. *Current Biology* 25: 2137–2142. https://doi.org/10.1016/j.cub.2015.06.047

Coates AG, Collins LS, Aubry MP, Berggren WA. 2004. The geology of the Darien, Panama, and the late Miocene-Pliocene collision of the Panama arc with

northwestern South America. *Geological Society of America Bulletin* 116: 1327–1344. https://doi.org/10.1130/B25275.1

Darriba D, Taboada G, Doallo R, Posada D.. 2012. jModelTest 2: more models, new heuristics and parallel computing. *Nature Methods* 9: 772. https://doi.org/10.1038/nmeth.2109

Dengo G. 1985. Mid America: Tectonic setting for the Pacific margin from southern México to northwestern Colombia, In: Nairn AEM, Stehli FG, Uyeda S. (Eds). *The Ocean Basins and Margins*. Springer, Boston, MA, 123–180. https://doi.org/10.1007/978-1-4613-2351-8_4

Ding L, Spicer RA, Yang J, Xu Q, Cai F, Li S, Lai Q, Wang H, Spicer TEV, Yue Y, Shukla A, Srivastava G, Ali Khan M, Bera S, Mehrotra R. 2017. Quantifying the rise of the Himalaya orogen and implications for the South Asian monsoon. *Geology* 45: 215–218. https://doi.org/10.1130/G38583.1

Eldredge N, Cracraft J. 1980. Phylogenetic Patterns and the Evolutionary Process. *Method and Theory in Comparative Biology*. Columbia university Press, New York. 329 pp. https://doi.org/10.1002/ajpa.1330610414

Fischer FCJ. 1962. Polycentropodidae, Psychomyidae. *Trichopterorum Catalogus III*. Nederlandsche Entomologische Vereeniging, Amsterdam, vi + 236 pp.

Flint OS Jr. 1967. Studies of Neotropical caddis flies, IV: new species from Mexico and Central America. *Proceedings of the United States National Museum* 123: 1–24. https://doi.org/10.5479/si.00963801.123-3619.1

Flint OS Jr. 1981. Studies of Neotropical caddisflies, XXVIII: the Trichoptera of the Rio Limón basin, Venezuela. *Smithsonian Contributions to Zoology* 330: 1–60. https://doi.org/10.5479/si.00810282.330

Goloboff PA. 1997. Self-weighted optimization: tree searches and character state reconstructions under implied transformation costs. *Cladistics* 13: 225–245. https://doi.org/10.1006/clad.1997.0043

Goloboff PA, Farris JS, Nixon KC. 2008. TNT, a free program for phylogenetic analysis. *Cladistics* 24: 774–786. https://doi.org/10.1111/j.1096-0031.2008.00217.x

Gorin VA, Solovyeva EN, Hasan M, Okamiya H, Karunarathna DMSS, Pawangkhanant P, de Silva A, Juthong W, Milto KD, Nguyen LT, Suwannapoom C, Haas A, Bickford DP, Das I, Poyarkov NA. 2020. A little frog

leaps a long way: compounded colonizations of the Indian Subcontinent discovered in the tiny Oriental frog genus Microhyla (Amphibia: Microhylidae). *PeerJ* 8: e9411.D. https://doi.org/ 10.7717/peerj.9411

Guitián J, Phelps S, Polissar PJ, Ausin B, Eglinton TI, Stoll HM. 2019. Mid-latitude temperature variations in the Oligocene to Early Miocene. *Paleoceanography and Paleoclimatology* 34(8): 1328–1343. https://doi.org/10.1029/2019PA003638

Guleria JS. 1992. Neogene vegetation of peninsular India. *Palaeobotanist* 40: 285–331.

Hall R. 2012. Late Jurassic–Cenozoic reconstructions of the Indonesian region and the Indian Ocean. *Tectonophysics* 570–571: 1–41. https://doi.org/10.1016/j.tecto.2012.04.021

Hauff F, Hoernle K, van den Bogaard P, Alvarado G, Garbe-Schönberg D. 2000. Age and geochemistry of basaltic complexes in western Costa Rica: contributions to the geotectonic evolution of Central America. *Geochemistry, Geophysics, Geosystems* 1: 1–41. https://doi.org/10.1029/1999GC000020

Hay WW. 2017. Toward understanding Cretaceous climate—An updated review. *Science China Earth Sciences* 60: 5–19. https://doi.org/10.1007/s11430-016-0095-9

Höhna S, Stadler T, Ronquist F, Britton T. 2011. Inferring speciation and extinction rates under different species sampling schemes. *Molecular Biology and Evolution* 28: 2577–2589. https://doi.org/10.1093/molbev/msr095

Holzenthal RW. 1988. Catalogo systematico de los Trichopteros de Costa Rica (Insecta: Trichoptera). *Brenesia.* 29: 51–82.

Holzenthal RW, Calor AR. 2017. Catalog of the Neotropical Trichoptera (Caddisflies). *ZooKeys* 654: 1–566. https://doi.org/10.3897/zookeys.654.9516

Jenkyns HC, Forster A, Schouten S, Damste JSS. 2004. High temperatures in the Late Cretaceous Arctic Ocean. *Nature*. 432: 888–892. https://doi.org/10.1038/nature03143

Katoh K, Standley DM. 2013. MAFFT Multiple Sequence Alignment Software Version 7: Improvements in Performance and Usability. *Molecular Biology and Evolution* 30(4): 772–780. https://doi.org/10.1093/molbev/mst010

Keppie DJ, Moán-Zenteno DJ. 2005. Tectonic Implications of Alternative Cenozoic Reconstructions for Southern Mexico and the Chortis Block. *International Geology Review* 47: 473–491. https://doi.org/0020-6814/05/801/473-19

Kimura M 1980. A simple method for estimating evolutionary rates of base substitutions through comparative studies of nucleotide sequences. *Journal of Molecular Evolution* 16(2): 111–120. https://doi.org/10.1007/BF01731581

Kirby MX, Jones DS, MacFadden BJ. 2008. Lower Miocene stratigraphyalong the Panama Canal and its bearing on the Central American Peninsula. *PLoSOne* 3: e2791 https://doi.org/10.1371/journal.pone.0002791

Klaus S, Morley RJ, Plathet M, Zhang Y, Li J. 2016. Biotic interchange between the Indian subcontinent and mainland Asia through time. *Nature Communications* 7(12132). https://doi.org/10.1038/ncomms12132

Kumar S, Stecher G, Li M, Knyaz C, Tamura K. 2018. MEGA X: Molecular Evolutionary Genetics Analysis across computing platforms. *Molecular Biology and Evolution.* 35:1547–1549. https://doi.org/10.1093/molbev/msy096

Lee MSY, Cau A, Naish D, Dyke GJ. 2014. Morphological clocks in paleontology, and a mid-Cretaceous origin of crown Aves. *Systematic Biology*. 63: 442–449. https://doi.org/10.1093/sysbio/syt110

Leigh EG, O ' Dea A, Vermeij GJ. 2013. Historical biogeography of the isthmus of Panama. *Biological Reviews*. 89:148 – 72. https://doi.org/10.1111/brv.12048.

Lepage T, Bryant D, Philippe H, Lartillot N. 2007. A general comparison of relaxed molecular clock models. *Molecular Bioliology and Evolution.* 24(12): 2669-80. https://doi.org/10.1093/molbev/msm193.

Lewis PO. 2001. A likelihood approach to estimating phylogeny from discrete morphological character data. *Systematic Biology.* 50: 913–925. https://doi.org/10.1080/106351501753462876

Lucena DAA., Almeida EAB. 2020. Morphology and Bayesian tip-dating recover deep Cretaceous-age divergences among major chrysidid lineages (Hymenoptera: Chrysididae). *Zoological Journal of the Linnean Society* XX, 1–44. https://doi.org/10.1093/zoolinnean/zlab010

Maes JM, Flint OS. 1988. Catalogo de los Trichoptera de Nicaragua. *Revista Nicaraguense de Entomologia* 2: 1–11.

Maes JM. 1999. Orden Trichoptera. In: Maes J-M (Ed) *Insectos de Nicaragua Catálogo de los Insectos y Artropodos Terrestres de Nicaragua Vol III*. Managua, Nicaragua, 1184–1199.

Malicky H. & Chantaramongkol P. 1992 Elf neue Köcherfliegen (Trichoptera) aus Thailand und angrenzenden Läden (Studien über thailädische Köcherfliegen Nr. 7). *Entomologische Zeitschrift mit Insecktenbörse* 101(5): 80–89.

Malm T, Johanson KA, Wahlberg N. 2013. The evolutionary history of Trichoptera (Insecta): A case of successful adaptation to life in freshwater. *Systematic Entomology*, 38: 459–473. https://doi.org/10.1111/syen.12016.

Mann P. 2007. Overview of the tectonic history of northern Central America. In: Mann, P, (Ed.), Geologic and tectonic development of the Caribbean plate boundary in northern Central America. *Geological Society of America Special Paper* 428: 1–19, https://doi.org/10.1130/2007.2428(01).

Mastretta-Yanes A, Moreno-Letelier A, Piñero D, Jorgensen HT, Emerson BC. 2015. Biodiversity in the Mexican highlands and the interaction of geology, geography and climate within the Trans-Mexican Volcanic Belt. *Journal of Biogeography* 42: 1586–1600. https://doi.org/10.1111/jbi.12546

Matzke NJ. 2014. Model selection in historical biogeography reveals that founder-event speciation is a crucial process in island clades. *Systematic Biology* 63: 951–970. https://doi.org/10.1093/sysbio/syu056

Mey W. 1998. Die Köcherfliegenfauna des Fan Si Pan-Massivs in Nord-Vietnam. 3. Beschreibung weiterer neuer Arten (Trichoptera). *Opuscula Zoologica Fluminensia* 165: 1–17.

Miller MA, Pfeiffer W, Schwartz T. 2010. Creating the CIPRES Science Gateway for inference of large phylogenetic trees. *Proceedings of the Gateway Computing Environments Workshop (GCE)*. New Orleans, Louisiana, p. 1–8.

Mirande MJ. 2009. Weighted parsimony phylogeny of the family Characidae (Teleostei: Characiformes). *Cladistics* 25: 574–613. https://doi.org/10.1111/j.1096-0031.2009.00262.x

Molineri C. 2006. Phylogeny of the mayfly family Leptohyphidae (Insecta: Ephemeroptera) in South America. *Systematic Entomology* 31: 711–728. https://doi.org/10.1111/j.1365-3113.2006.00357.x

Montes C, Cardona A, McFadden R, Morón SE, Silva CA, Restrepo-Moreno S, Ramírez DA, Hoyos N, Wilson J, Farris D, Bayona GA, Jaramillo CA, Valencia V, Bryan J, Flores JA. 2012. Evidence for middle Eocene and younger land emergence in Central Panama: implications for isthmus closure. *Geological Society of America Bulletin* 124: 780–99. https://doi.org/10.1130/B30528.1.

Montes C, Cardona A, Jaramillo C, Pardo A, Silva JC, Valencia V, Ayala C, Pérez-Angel LC, Rodriguez-Parra LA, Ramirez V, Niño H. 2015. Middle Miocene closure of the Central American Seaway. *Science* 348: 226–229. https://doi.org/10.1126/science.aaa2815

Morley RJ. 2018. Assembly and division of the South and South-East Asian flora in relation to tectonics and climate change. *Journal of Tropical Ecology* 34: 209–234. https://doi.org/10.1017/S0266467418000202

Morse JC. 2021. Trichoptera World Checklist. Available at: http://www.clemson.edu /cafls/departments/esps/database/trichopt/index.htm (accessed in may. 2021).

Mosely ME. 1934. Some new exotic Trichoptera. *Stylops* 3: 139–142. https://doi.org/10.1111/j.1365-3113.1934.tb01566.x

Mosely ME. 1948. Trichoptera. Expedition to South-West Arabia 1937-8. *British Museum (Natural History)* 1: 67–86.

Mosely ME, Kimmins DE. 1953. *The Trichoptera of Australia and New Zealand*. Trustees of the British Museum (Natural History), London. https://doi.org/10 .5962/bhl.title.118696

Moulton SR II, Stewart KW. 1997. A new species and first record of the caddisfly genus Cnodocentron Schmid (Trichoptera: Xiphocentronidae) north of Mexico. In: Holzenthal RW, Flint OS, Jr. (Eds) *Proceedings of the 8th International Symposium on Trichoptera*. Ohio Biological Survey, Columbus, Ohio, 343–347.

Muñoz-Quesada F. 2000. Especies del orden Trichoptera (Insecta) en Colombia. *Biota Colombiana* 1: 267–288.

Nielsen A. 1957. A comparative study of the genital segments and their appendages in male Trichoptera. *Biologiske Skrifter, Danske Videnskabernes Selskab* 8(5): 1–159.

Nielsen A. 1980 A comparative study of the genital segments and the genital chamber in female Trichoptera. *Kongelige Danske Videnskabernes Selskab Biologiske Skrifter* 23: 1–200.

Nixon KC. 2002. WinClada, Version 1.00.08. Published by the author: Ithaca, NY, USA. Available at: http://www.diversityoflife.org/winclada/

O'Dea A, Lessios HA, Coates AG, Eytan RI, Restrepo-Moreno SA, Cione AL, Collins LS, de Queiroz A, Farris DW, Norris RD, Stallard RF, Woodburne MO, Aguilera O, Aubry MP, Berggren WA, Budd AF, Cozzuol MA, Coppard SE, Duque-Caro H, Finnegan S, Gasparini GM, Grossman EL, Johnson KG, Keigwin LD, Knowlton N, Leigh EG, Leonard-Pingel JS, Marko PB, Pyenson ND, Rachello-Dolmen PG, Soibelzon E, Soibelzon L, Todd JA, Vermeij GJ, Jackson JBC. 2016. Formation of the Isthmus of Panama. *Science Advances* 2: e1600883. https://doi.org/10.1126/sciadv.1600883

Oláh J, Johanson KA. 2007. Trinominal terminology for cephalic setose warts in Trichoptera (Insecta). *Braueria* 34: 43–50.

Oláh J, Johanson KA. 2010. New Xiphocentronidae species from Vietnam (Insecta, Trichoptera). *Denisia* 29: 243-275.

Prather AL. 2003. Revision of the Neotropical caddisfly genus *Phylloicus* (Trichoptera: Calamoceratidae). *Zootaxa* 275: 1–214. https://doi.org/10.11646/zootaxa.275.1.1

Pyron RA. 2011. Divergence time estimation using fossils as terminal taxa and the origins of Lissamphibia. *Systematic Biology*. 60: 466–481. https://doi.org/10.1093/sysbio/syr047

Quade J, Cerling T, Bowman J. 1989. Development of Asian monsoon revealed by marked ecological shift during the latest Miocene in northern Pakistan. *Nature* 342: 163–166. https://doi.org/10.1038/342163a0

Rambaut A. 2016. FigTree: Tree Figure Drawing Tool, version 1.4.3. Available at: http://tree.bio.ed.ac.uk.

Rambaut A, Drummond AJ, Xie D, Baele G, Suchard MA. 2018. Posterior summarisation in Bayesian phylogenetics using Tracer 1.7. *Systematic Biology*. syy032. https://doi.org/10.1093/sysbio/syy032

Ree RH, Smith SA. 2008. Maximum likelihood inference of geographic range evolution by dispersal, local extinction, and cladogenesis. *Systematic Biology* 57: 4–14. https://doi.org/10.1080/10635150701883881

Ronquist F, Klopfstein S, Vilhelmsen L, Schulmeister S, Murray DL, Rasnitsyn AP. 2012a. A total-evidence approach to dating with fossils, applied to the early radiation of the Hymenoptera. *Systematic Biology* 61: 973–999. https://doi.org/10.1093/sysbio/sys058.

Ronquist F, Teslenko M, Mark P van der, Ayres DL, Darling A, Höhna S, Larget B, Liu L, Suchard MA, Huelsenbeck JP. 2012b. MrBayes 3.2: efficient Bayesian phylogenetic inference and model choice across a large model space. *Systematic Biology* 61: 539–542. https://doi.org/10.1093/sysbio/sys029

Rosa BB, Melo GAR, Barbeitos MS. 2019. Homoplasy-based partitioning outperforms alternatives in Bayesian analysis of discrete morphological data. *Systematic Biology* 68: 657–671. https://doi.org/10.1093/sysbio/syz001

Ross HH. 1949. Xiphocentronidae, a new family of Trichoptera. *Entomological news* 60: 1–7.

Ruiter DE. 2006. The female of *Cnodocentron* (*Caenocentron*) *yavapai* Moulton and Stewart (Trichoptera: Xiphocentronidae). *Western North American Naturalist* 66: 527–528. https://doi.org/10.3398/1527-0904(2006)66[527:TFOCCY]2.0.CO;2

Sanmartín I. 2012. Historical Biogeography: Evolution in Time and Space. *Evolution: Education and Outreach* 5: 555–568. https://doi.org/10.1007/s12052-012-0421-2

Sanmartín I, Enghoff H, Ronquist F. 2001. Patterns of animal dispersal, vicariance and diversification in the Holarctic. *Biological Journal of the Linnean Society* 73(4): 345–390. https://doi.org/10.1006/bijl.2001.0542

Schaaf P, Moran-Zenteño D, Hernandez-Bernal M, Solis-Pichardo G, Tolson G, Kohler H. 1995. Paleogene continental margin truncation in southwestern Mexico: Geochronological evidence. *Tectonics* 14: 1339–1350. https://doi.org/10.1029/95TC01928.

Schmid F. 1982. La famille des Xiphocentronidae (Trichoptera: Annulipalpia). *Mémoires de la Sociét Entomologique du Canada* 121: 1–127. https://doi.org/10.4039/entm114121fv

Silva-Romo G, Mendoza-Rosales CC, Campos-Madrigal E, Hernández-Marmolejo YB, Rosa-Mora OA, Torre-González AI, Bonifacio-Serralde C, López-García N, Nápoles-Valenzuela JI. 2018. Timing of the Cenozoic basins of Southern Mexico and its relationship with the Pacific truncation process: Subduction erosion or

detachment of the Chortís block, *Journal of South American Earth Sciences* 83: 178–194. https://doi.org/10.1016/j.jsames.2018.01.007

Songtham W, Ratanasthien B, Mildenhall DC, Singharajwarapan S, Kandharosa W. 2003. Oligocene-Miocene climatic changes in northern Thailand resulting from extrusion tectonics of Southeast Asian landmass. *ScienceAsia* 29(3): 221–233. https://doi.org/10.2306/scienceasia1513-1874.2003.29.221

Srivastava G, Paudayal KN, Utescher T, Mehrotra RC. 2018. Miocene vegetation shift and climate change: evidence from the Siwalik of Nepal. *Global and Planetary Change* 161: 108–120.

Thomas JA, Frandsen PB, Prendini E, Zhou X, Holzenthal RW. 2020. A multigene phylogeny and timeline for Trichoptera (Insecta). *Systematic Entomology,* 45 (3), 670–686. https://doi.org/10.1111/syen.12422

Tiffney, BH. 1985. The Eocene North Atlantic land bridge: its importance in Tertiary and modern phytogeography of the Northern Hemisphere. *Journal of the Arnold Pamphilis Arboretum* 66: 243–273.

Ulmer G. 1906. Neuer beitrag zur kenntnis aussereuropäischer Trichopteren. *Notes from the Leyden Museum* 28: 1–116.

Vaidya G, Lohman DJ, Meier R. 2011. SequenceMatrix: concatenation software for the fast assembly of multi-gene datasets with character set and codon information. *Cladistics* 27(2): 171–180. https://doi.org/10.1111/j.1096-0031.2010.00329.x

Vilarino A, Bispo PC. 2020. New records and two new species of *Xiphocentron* Brauer 1870 (Trichoptera, Xiphocentronidae) from southern Atlantic Forest, Brazil. *Zootaxa* 4851(2): 386–400. https://doi.org/10.11646/zootaxa.4851.2.11

Vilarino A, Calor AR. 2015. New species of *Xiphocentron* Brauer 1870 (Trichoptera: Xiphocentronidae) from Northeastern Brazil. *Zootaxa* 3914 (1): 46–54. https://doi.org/10.11646/zootaxa.3914.1.2

Wichard W, Kraemer MMS, Luer C. 2006. First caddisfly species from Mexican amber (Insecta: Trichoptera). *Zootaxa* 1378: 37–48. https://doi.org/10.11646/zootaxa.1378.1.3

Wright DF. 2017. Bayesian estimation of fossil phylogenies and the evolution of early to middle Paleozoic crinoids (Echinodermata). *Journal of Paleontology* 91: 799–814. https://doi.org/10.1017/jpa.2016.141

Yu Y, Blair C, He XJ. 2020. RASP 4: Ancestral State Reconstruction Tool for Multiple Genes and Characters. *Molecular Biology and Evolution* 37(2): 604–606. https://doi.org/10.1093/molbev/msz257

Zachos J, Pagani M, Sloan L, Thomas E, Billups K. 2001. Trends, rhythms, and aberrations in global climate 65 Ma to present. *Science* 292(5517): 686–693. https://doi.org/686-693,10.1126/science.1059412

Zhang C. 2019. Molecular clock dating using MrBayes. *Vertebrata PalAsiatica* 57(3): 241–252. https://doi.org/10.19615/j.cnki.1000-3118.190408

Zhang C, Stadler T, Klopfstein S, Heath TA, Ronquist F. 2016. Total-evidence dating under the fossilized birth–death process. *Systematic Biology* 65(2): 228–249. https://doi.org/10.1093/sysbio/syv080

FIGURES

Figure 1. Xiphocentronidae world distribution showing *Cnodocentron* species distribution in red circles. Tropical moist forests are displayed in green.

Figure 2. A, Wing pattern of *C.* (*Caenocentron*) *trilineatum*. B, Sternum V of *C.* (*Caenocentron*) *carlosdelarosai* sp. nov. showing reticulate cuticular plate at 200x. C, abdomen of *C.* (*Caenocentron*) *carlosdelarosai* sp. nov., 80x. D, Sternum V of *Melanotrichia samaconius*.

Figure 3. Mesothorax: A, *C.* (*Caenocentron*) *carlosdelarosai* sp. nov.; B, *C.* (*Cnodocentron*) *brogimarus*; C, *Xiphocentron maiteae*; D, *Melanotrichia samaconius*. Hind leg apical spur: E, *Drepanocentron* sp.; F, *Cnodocentron* sp.

Figure 4. Wing venation: A, *Melanotrichia attia*; B, *C.* (*Cnodocentron*) *tchaturbhuja*; C, *C.* (*Cnodocentron*) *girika*. Male genitalia: D, aspect of mesal sclerite of *Melanotrichia* sp., 200x; E, *Melanotrichia* attia, lateral view; F, *C.* (*Cnodocentron*) *vrisaparvan*, lateral view. Male genitalia, sternum IX, ventral: G, *C. filamenta*; H, *C. brogimarus*; I, *C. tchaturbhuja*; J, *C. devayani*; K, *C. vrisaparvan*; L, *C. girika*. Female genitalia, segment VIII apex, dorsal: M, *C.* (*Caenocentron*) *carlosdelarosai* sp. nov.; N, *C.* (*Cnodocentron*) *tchaturbhuja*.

Figure 5. Maximum credibility Bayesian tree obtained from 46 morphological characters and COI coded to *Cnodocentron* sensu Schmid and related taxa. (all compatible groups shown). Morphological character states are displayed along the branches: Boxes refer to unambiguous transformations, circles to characters under ACCTRAN optimization. Black symbols indicate unique character changes. Posterior probability support values are displayed in boxes below the node branches. Male genitalia of species of each clade are displayed in lateral view, Oriental species modified from the original descriptions: Malicky & Chantaramongkol (1992), Oláh & Johanson (2010), Schmid (1982).

Figure 6. Chronogram resulted from Bayesian analysis employing a relaxed clock. Most likely ancestral distribution recovered in DEC analysis and estimated mean age are displayed at the nodes. Dispersal events are indicated as a black line below the distribution boxes, vicariant events are indicated in a green line, as recovered in the biogeographic analysis. Highest posterior density (HPD) 95% intervals for the ages of the nodes are indicated by light blue bars. Timescale and global surface temperature estimated from $\delta^{18}O$ benthic (Zachos *et al.* 2001) are displayed on the bottom. Eocene and Miocene thermal optimum are highlighted in gray. *Cnodocentron* and *Caenocentron* species distributions are shown in the maps.

Figure 7. *Caenocentron carlosdelarosai* sp. nov. A, head and thorax; B, wing venation.

Figure 8. *Caenocentron carlosdelarosai* sp. nov. male genitalia. A, lateral; B, dorsal; C, ventral.

Figure 9-11. *Caenocentron* female genitalia. **9.** *Caenocentron carlosdelarosai* sp. nov. A, lateral; B, dorsal; C, detail of apex lateral; D, detail of apex ventral. **10.** *Caenocentron rafamoralesi* sp. nov. A, lateral; B, dorsal; C, detail of apex lateral; D, detail of apex ventral. **11.** *Caenocentron yavapai* A, lateral; B, dorsal; C, detail of apex ventral (modified from Ruiter 2006). Scale bar = 0.1mm.

Figure 12. Bayesian analysis of COI sequences of *Caenocentron carlosdelarosai* sp. nov. and *Caenocentron rafamoralesi* sp. nov. and other xiphocentronids, showing clustering associating male and females of each species. Blue color = *Caenocentron carlosdelarosai* sp. nov.; yellow color = *Caenocentron rafamoralesi* sp. nov.; COI accession numbers are displayed in front of each specimen. Posterior probability values are displayed above each node.

Figure 13. *Caenocentron rafamoralesi* sp. nov. A, Wing venation. Male genitalia B, lateral; C, dorsal; D, ventral.

Figure 14. *Caenocentron yavapai* (Moulton & Stewart, 1997) male genitalia: A, lateral; B, dorsal; C, ventral.

Figure 15. *Caenocentron galesus* (Schmid, 1982), male genitalia A, lateral; B, ventral.

Figure 16. *Caenocentron ideolus* (Schmid, 1982), male genitalia: A, lateral; B, ventral.

Figure 17. *Caenocentron immaculatum* (Flint, 1991), male genitalia: A, lateral; B, dorsal; C, ventral.

Figure 18. *Caenocentron lausus* (Schmid, 1982), male genitalia: A, lateral; B, ventral.

Figure 19. *Caenocentron pallas* (Schmid, 1982). A, Wing venation. Male genitália: B, lateral; C, dorsal; D, ventral.

Figure 20. *Caenocentron trilineatum* (Mosely, 1934). A, Wing venation. Male genitalia: B, lateral; C, dorsal; D, ventral; E, detail paraproct lateral; F, phallus apex lateral and ventral, respectively.

Figure 21. Paleogeography of Southeast Asia and Mesoamerica: A, Southeast Asia, showing the collision of Indian plate and Asia. B, Mesoamerica showing the southward movement of Chortis block. Dispersal and vicariant events with their respective mean ages are displayed as arrows and dotted lines, respectively. Montane regions are in dark gray. Whitish regions indicate progressive seasonal dry climates after the Middle Miocene. Paleogeographic reconstructions of Mesoamerica modified from Keppie & Zenteno (2005) and interpreted from evidences presented by Kirby *et al.* (2008), Coates *et al.* (2004) and Montes *et al.* (2012). Reconstructions of Southeast Asia modified after Morley (2018) and Gorin *et al.* (2020).

Table 1. Species included in the phylogenetic analyses, with respective indication of locality, depository collection (or literature source) and sex of the individuals.

Genera	Species	Locality	Collection / Source	Sex
Cnodo. (Cnodocentron)	*brogimarus*	Thailand, Tung Yaw	MZSP	♂
"	*devayani*	India, Assam	Schmid 1982	♂
"	*filamenta*	Vietnam	Oláh & Johanson 2010	♂
"	*girika*	India, Assam	Schmid 1982	♂
"	*tchaturbhuja*	India, Sikkim, Tikjak	CNC165709	♂, ♀
"	*vrisaparvan*	Assam, Rupa	CNC165711	♂, ♀
Cnodo. (Caenocentron)	*carlosdelarosai*	Costa Rica, Guanacaste	BIOUG	♂, ♀
"	*galesus*	Costa Rica	USNMENT01028602	♂
"	*ideolus*	Mexico, Lomas de Chapultepec	Schmid 1982	♂
"	*immaculatum*	Colombia, Dpto. Antioquia	USNM	♂
"	*lausus*	Nicaragua, Villa Somoza	USNM	♂
"	*pallas*	Panama, Canal Zone, Gamboa	USNM	♂
"	*rafamoralesi*	Costa Rica, Guanacaste	BIOUG	♂, ♀
"	*trilineatum*	El Salvador	USNM	♂
"	*yavapai*	Arizona, Yavapai Co., Bubbling Springs	UMSP000021747	♂, ♀
Outgroups				
Drepanocentron	*vang*	Vietnam	MZSP	♂, ♀
Melanotrichia	*attia*	Thailand	MZSP	♂, ♀
"	*attiaides*	Thailand	MZSP	♂
"	*samaconius*	Indonesia, Jawa	MZSP	♂
Xiph. (Xiphocentron)	*aureum*	Panama	UMSP171589	♂, ♀
Xiph. (Glyphocentron)	*euryale*	Costa Rica	USNMENT01028621	♂
Xiph. (Rhamphocentron)	*messapus*	United States, Texas	USNM	♂
Xiph. (Antillotrichia)	*haitiense*	Haiti, Camp Perin, Haiti	USNM	♂
"	*maeteae*	Brazil, Bahia	UFBA	♂
"	*mnesteus*	Venezuela, Barinitas	USNMENT01028619	♂

Table 2. Morphological data matrix. "?" represents missing data; "-" represents inapplicable characters.

Taxon	**000000001**	**1111111112**	**2222222223**	**3333333334**	**444444**
Charater	**1234567890**	**1234567890**	**1234567890**	**1234567890**	**123456**
Drepanocentron vang	0110100110	0100000001	0100010100	0-10---011	021102
Melanotrichia attia	0000000000	00--001100	01100200--	0-0----011	101001
Melanotrichia samaconius	0000000000	00--001100	01100100--	0-0----00-	--1100
Melanotrichia attiaides	0000000000	00--001100	01100200--	0-0----011	101001
X. (*Rhamphocentron*) *messapus*	?110100110	10--000000	01000100--	0-10---011	001102
X. (*Xiphocentron*) *aureum*	0110100110	1100000000	01000100--	0-0----00-	--1011
X. (*Glyphocentron*) *euryale*	?101100100	10--000011	01011100--	0-10---00-	--1110
X. (*Antillotrichia*) *maiteae*	?101101100	10--000100	01010100--	100-00000-	--0---
X. (Antillotrichia) mnesteus	?101100100	10--000100	11010100--	0-10---10-	--1102
X. (Antillotrichia) haitiensis	?101100100	00--001100	01010200--	0-10---110	001100
C. (Cnodocentron) girika	??00000000	1011001000	01001100--	110-001110	201110
C. (Cnodocentron) brogimarus	?000110000	1101101000	01000201--	110-01100-	--1210
C. (Cnodocentron) tchaturbhuja	1000111000	1101100000	01001200--	110-001011	011202
C. (Cnodocentron) vrisaparvan	1000000000	1111001000	01001200--	110-00100-	--1110
C. (Cnodocentron) filamenta	??0?111000	1100100000	01000000--	110-01100-	--1202
C. (Cnodocentron) devayani	??0?000000	1110000000	00000200--	110-001011	001210
C. (Caenocentron) yavapai	0101100102	0100000001	0101011110	111111011-	--0---
C. (Caenocentron) rafamoralesi sp.n.	0101100102	0100000000	0000011100	111100110-	--1102
C. (Caenocentron) carlosdelarosai sp.n.	?101100101	10--010000	1001101110	111210010-	--0---
C. (Caenocentron) pallas	?101100101	10--010001	0001101111	1112000111	000---
C. (Caenocentron) immaculatum	?101100101	10--010000	1001101111	111210010-	--1010
C. (Caenocentron) lausus	?101100101	10--010000	1001101110	111210010-	--1010
C. (Caenocentron) trilineatum	?101100101	10--010001	1001101110	111210110-	--0---
C. (Caenocentron) ideolus	??01100101	10--010011	1001101110	111110110-	--1010
C. (Caenocentron) galesus	?101100101	10--010000	1001101111	111210010-	--0---

Table 3. Sequences of COI barcode used in the phylogenetic inference, and respective BOLD accession number.

Species	BOLD accession number
Drepanocentron dentatum	GENCO078-19|
Melanotrichia samaconius	HMKKT894-11|
Xiphocentron aureum	KKCAD140-07|
Xiphocentron mnesteus	KKUMN399-10|
Xiphocentron haitiense	OFTRI450-10
Cnodocentron trilineatum	SICOB516-18
Cnodocentron rafamoralesi sp. nov.	GMCEB2330-18
Cnodocentron carlosdelarosai sp. nov.	GMAAH1005-16

Table 4. Morphological partitions used for the Bayesian inferences. The partitions were established based on its levels of homoplasy obtained from consistence index of a cladistic analysis with implied weight of characters. Some individual values were combined into more inclusive classes.

Partition	Consistency index	Characters
01	1	1, 2, 3, 4, 6, 8, 9, 10, 15, 16, 23, 27, 29, 30, 32;
02	2	5, 7, 13, 18, 19, 24, 34, 35, 40, 41, 42;
03	2.75	31, 33, 36, 37, 38, 14, 22, 28;
04	3.0–3.2	21, 17, 25;
05	3.5	11, 43;
06	3.7 – 4.0	12, 20, 44, 45, 39;
07	5.2–5.5	26, 46.

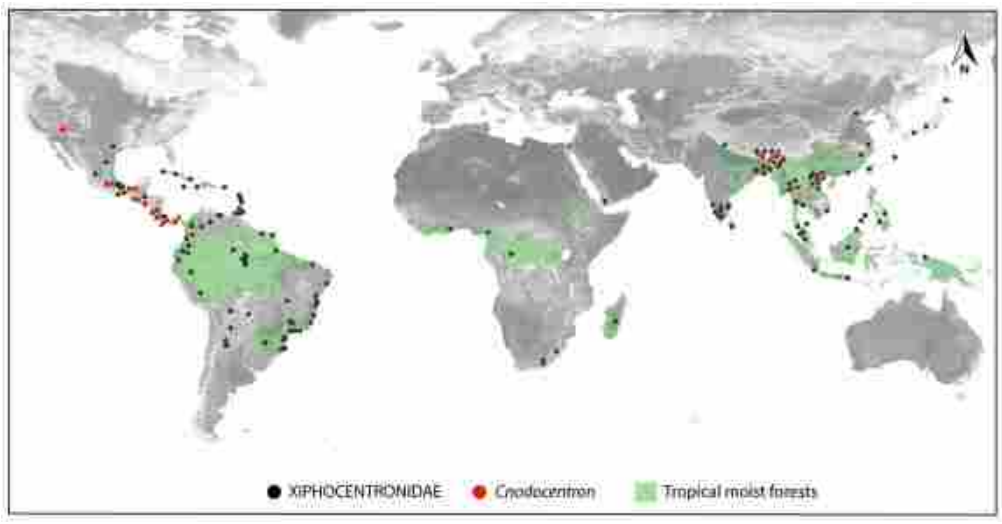

Figure 1. Xiphocentronidae world distribution showing Cnodocentron species distribution in red circles. Tropical moist forests are displayed in green.

243x126mm (600 x 600 DPI)

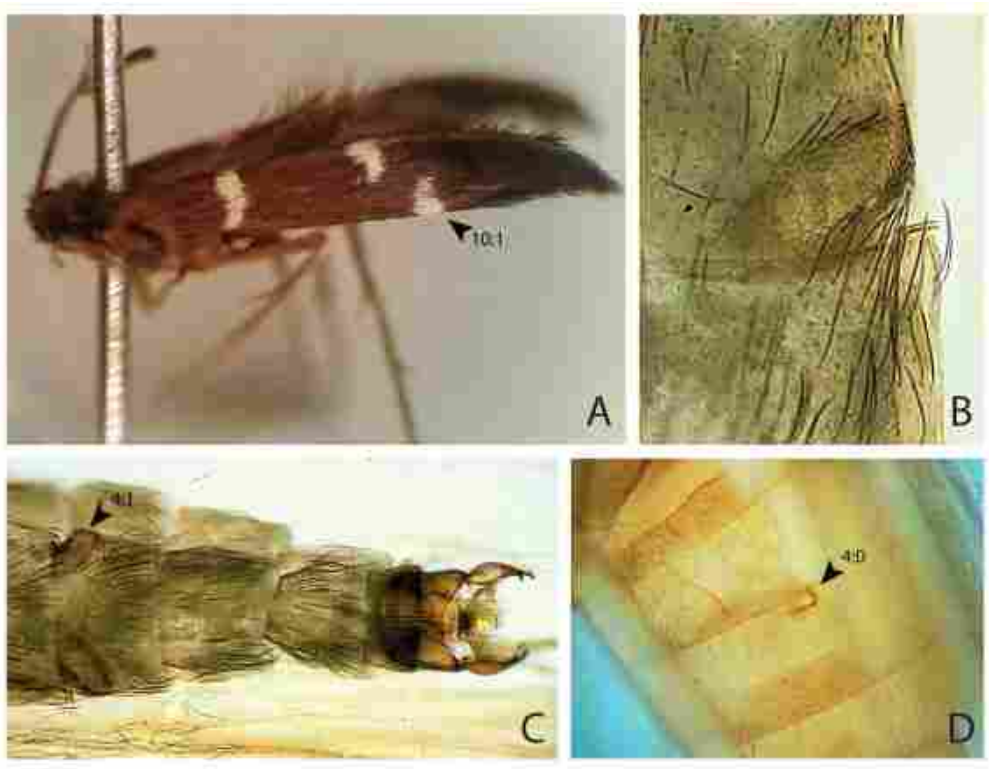

Figure 2. A, Wing pattern of C. (Caenocentron) trilineatum. B, Sternum V of C. (Caenocentron) carlosdelarosai sp. nov. showing reticulate cuticular plate at 200x. C, abdomen of C. (Caenocentron) carlosdelarosai sp. nov., 80x. D, Sternum V of Melanotrichia samaconius.

182x139mm (600 x 600 DPI)

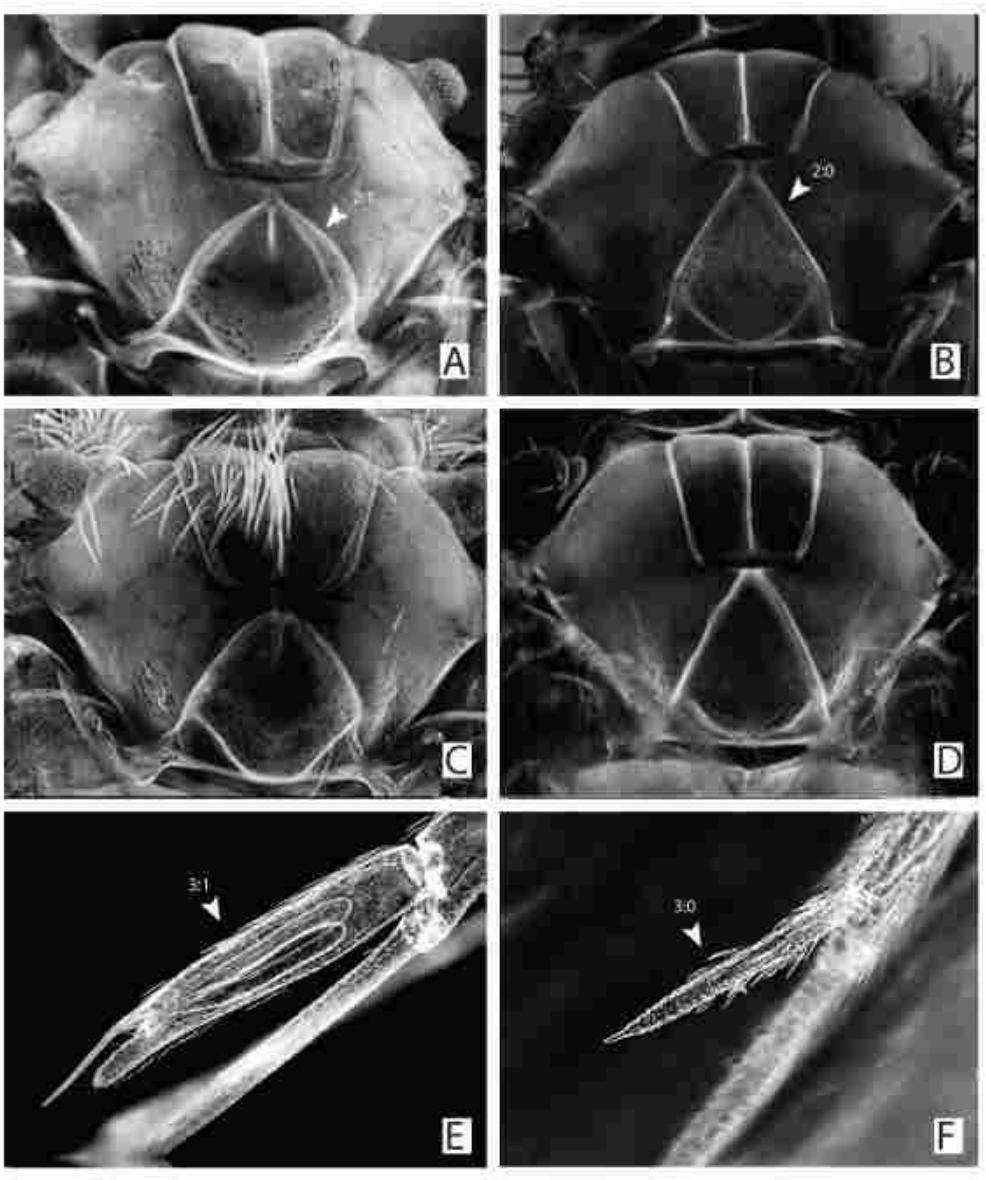

Figure 3. Mesothorax: A, C. (Caenocentron) carlosdelarosai sp. nov.; B, C. (Cnodocentron) brogimarus; C, Xiphocentron maiteae; D, Melanotrichia samaconius. Hind leg apical spur: E, Drepanocentron sp.; F, Cnodocentron sp.

193x227mm (300 x 300 DPI)

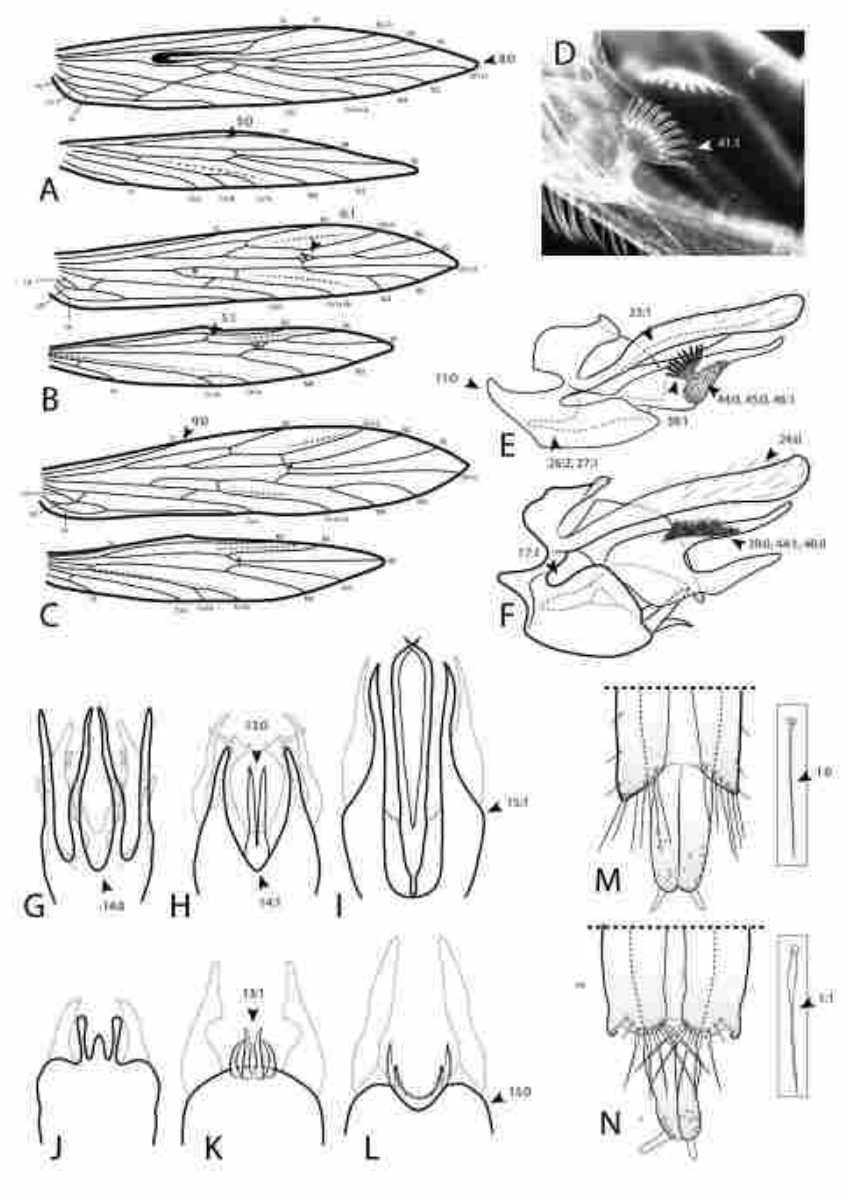

Figure 4. Wing venation: A, Melanotrichia attia; B, C. (Cnodocentron) tchaturbhuja; C, C. (Cnodocentron) girika. Male genitalia: D, aspect of mesal sclerite of Melanotrichia sp., 200x; E, Melanotrichia attia, lateral view; F, C. (Cnodocentron) vrisaparvan, lateral view. Male genitalia, sternum IX, ventral: G, C. filamenta; H, C. brogimarus; I, C. tchaturbhuja; J, C. devayani; K, C. vrisaparvan; L, C. girika. Female genitalia, segment VIII apex, dorsal: M, C. (Caenocentron) carlosdelarosai sp. nov.; N, C. (Cnodocentron) tchaturbhuja.

210x296mm (300 x 300 DPI)

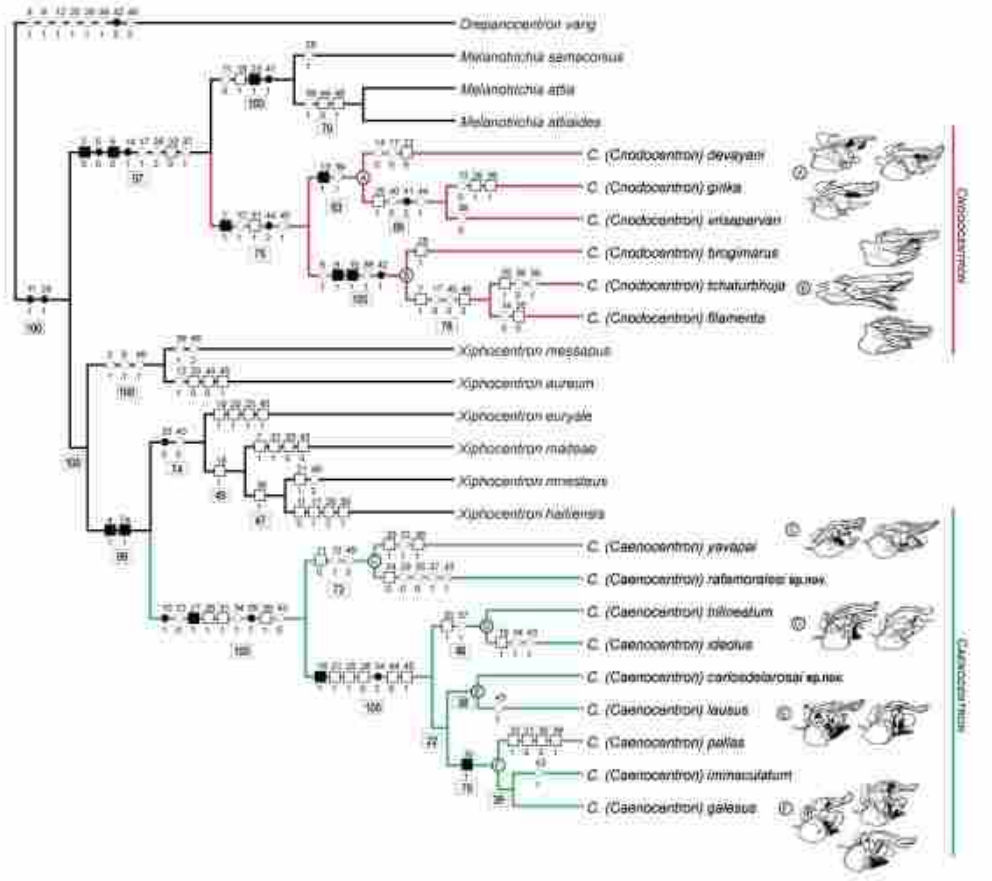

Figure 5. Maximum credibility Bayesian tree obtained from 46 morphological characters and COI coded to Cnodocentron sensu Schmid and related taxa. (all compatible groups shown). Morphological character states are displayed along the branches: Boxes refer to unambiguous transformations, circles to characters under ACCTRAN optimization. Black symbols indicate unique character changes. Posterior probability support values are displayed in boxes below the node branches. Male genitalia of species of each clade are displayed in lateral view, Oriental species modified from the original descriptions: Malicky & Chantaramongkol (1992), Oláh & Johanson (2010), Schmid (1982).

299x284mm (300 x 300 DPI)

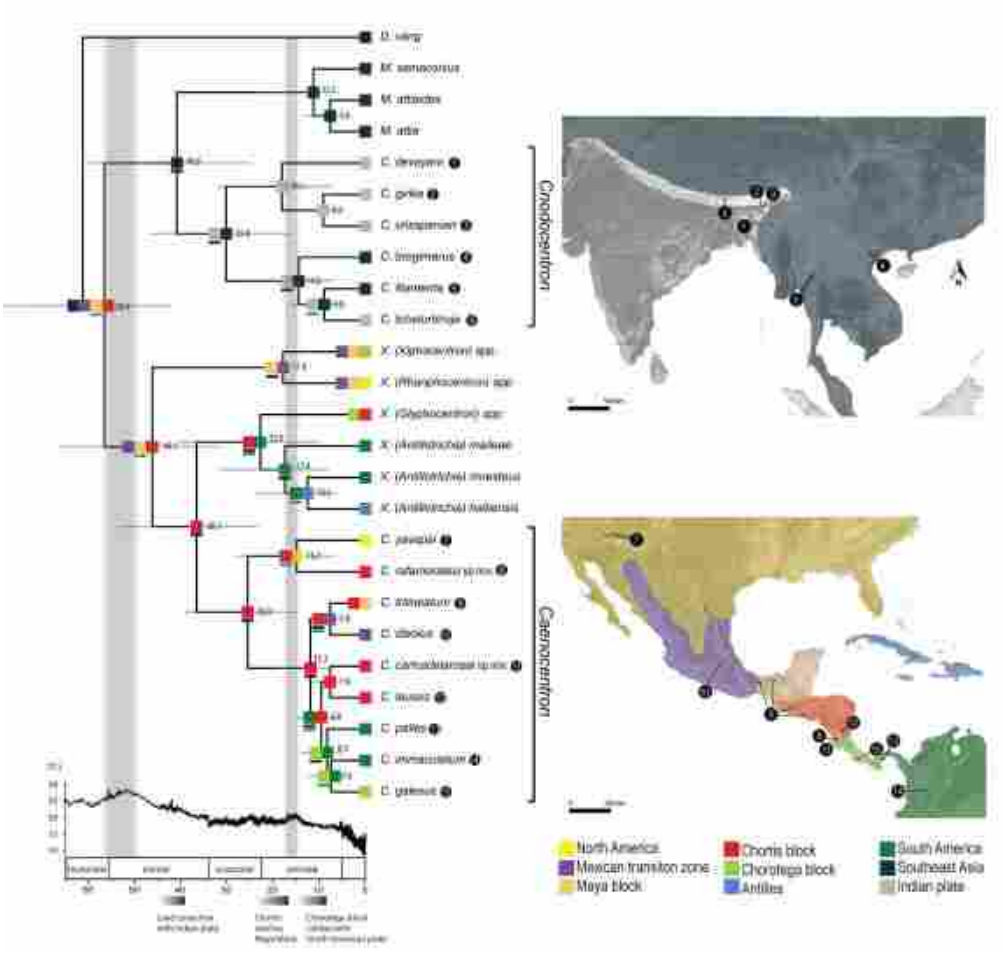

Figure 6. Chronogram resulted from Bayesian analysis employing a relaxed clock. Most likely ancestral distribution recovered in DEC analysis and estimated mean age are displayed at the nodes. Dispersal events are indicated as a black line below the distribution boxes, vicariant events are indicated in a green line, as recovered in the biogeographic analysis. Highest posterior density (HPD) 95% intervals for the ages of the nodes are indicated by light blue bars. Timescale and global surface temperature estimated from δ18O benthic (Zachos et al. 2001) are displayed on the bottom. Eocene and Miocene thermal optimum are highlighted in gray. Cnodocentron and Caenocentron species distributions are shown in the maps.

360x349mm (300 x 300 DPI)

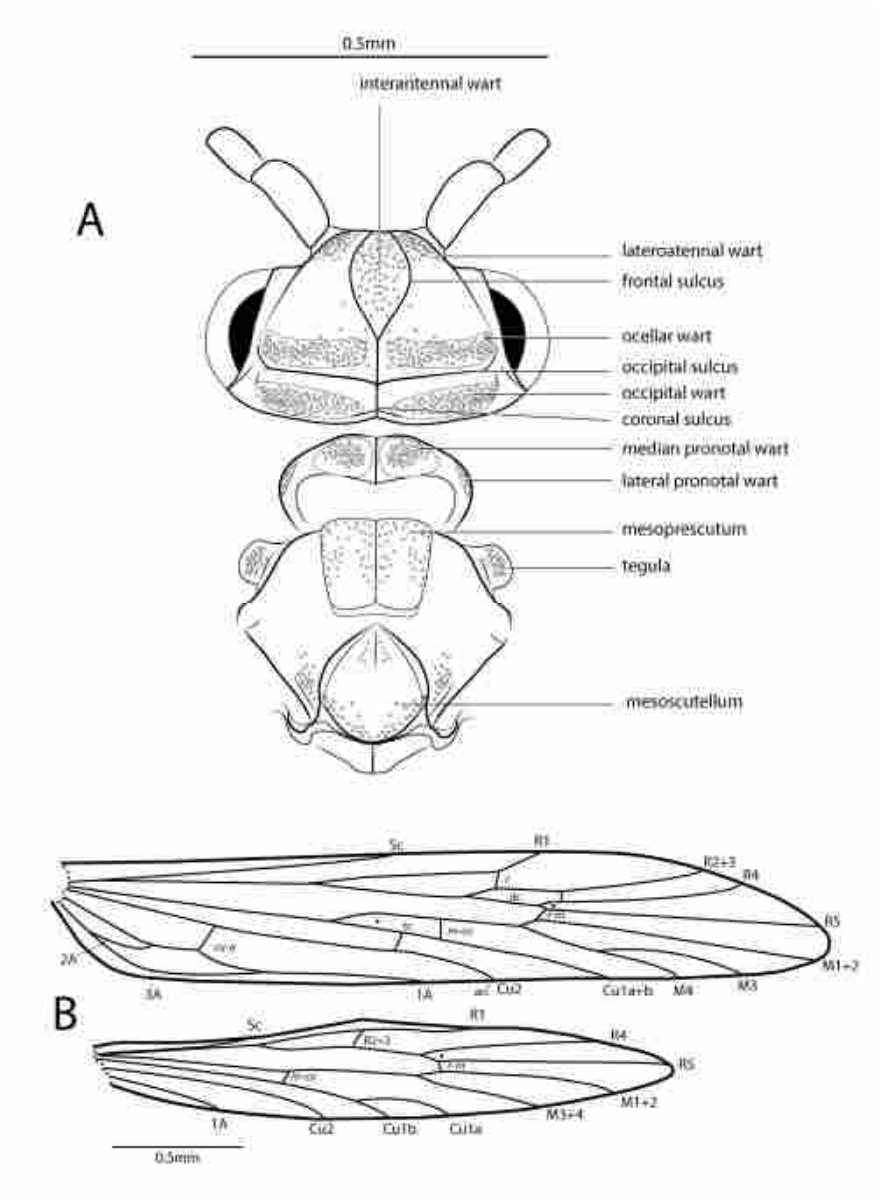

Figure 7. Caenocentron carlosdelarosai sp. nov. A, head and thorax; B, wing venation.

316x432mm (300 x 300 DPI)

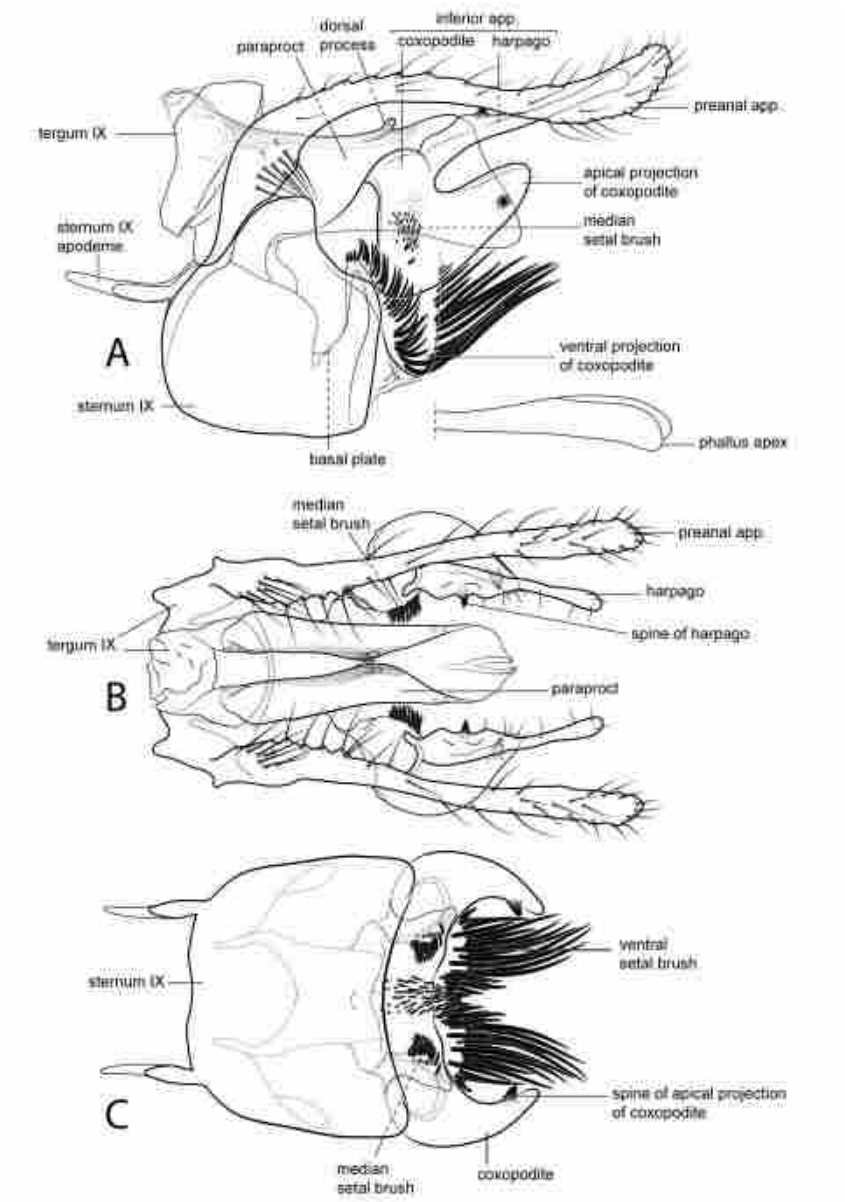

Figure 8. Caenocentron carlosdelarosai sp. nov. male genitalia. A, lateral; B, dorsal; C, ventral.

337x482mm (300 x 300 DPI)

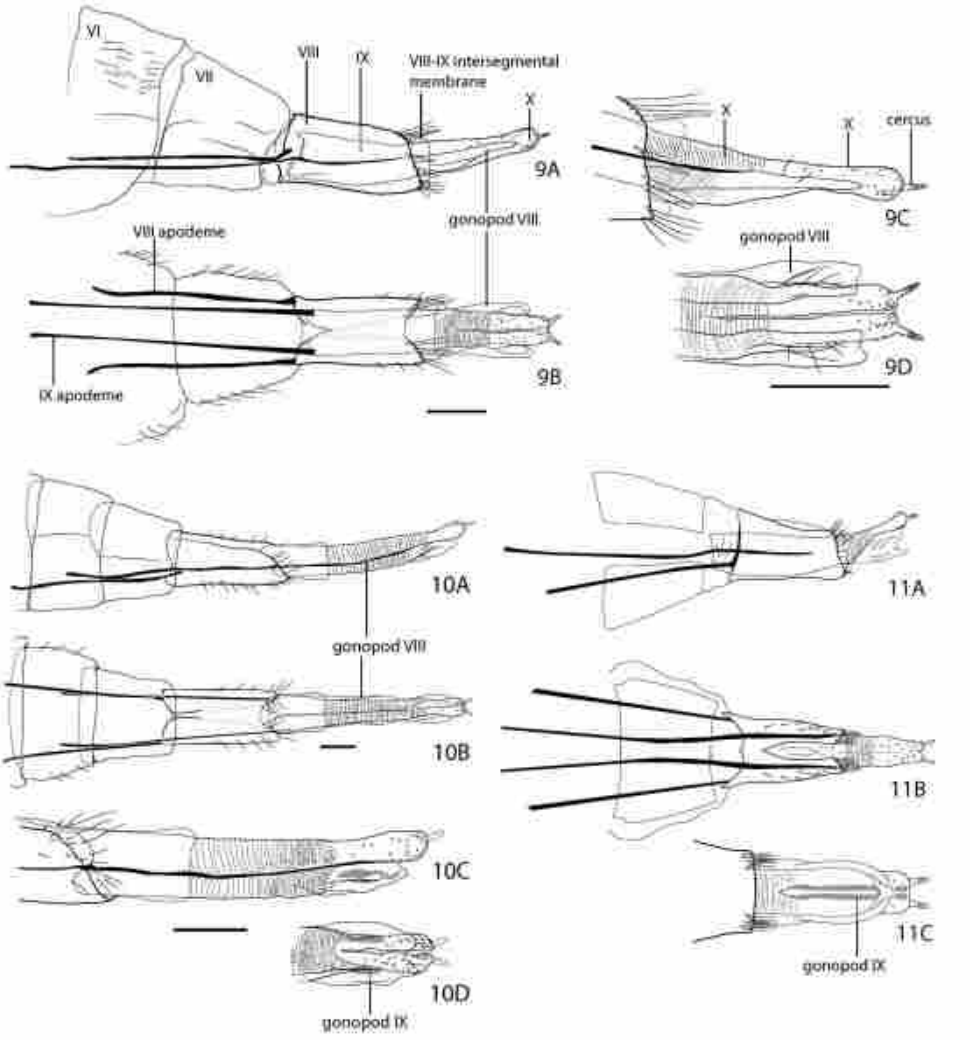

Figure 9-11. Caenocentron female genitalia. 9. Caenocentron carlosdelarosai sp. nov. A, lateral; B, dorsal; C, detail of apex lateral; D, detail of apex ventral. 10. Caenocentron rafamoralesi sp. nov. A, lateral; B, dorsal; C, detail of apex lateral; D, detail of apex ventral. 11. Caenocentron yavapai A, lateral; B, dorsal; C, detail of apex ventral (modified from Ruiter 2006). Scale bar = 0.1mm.

201x221mm (300 x 300 DPI)

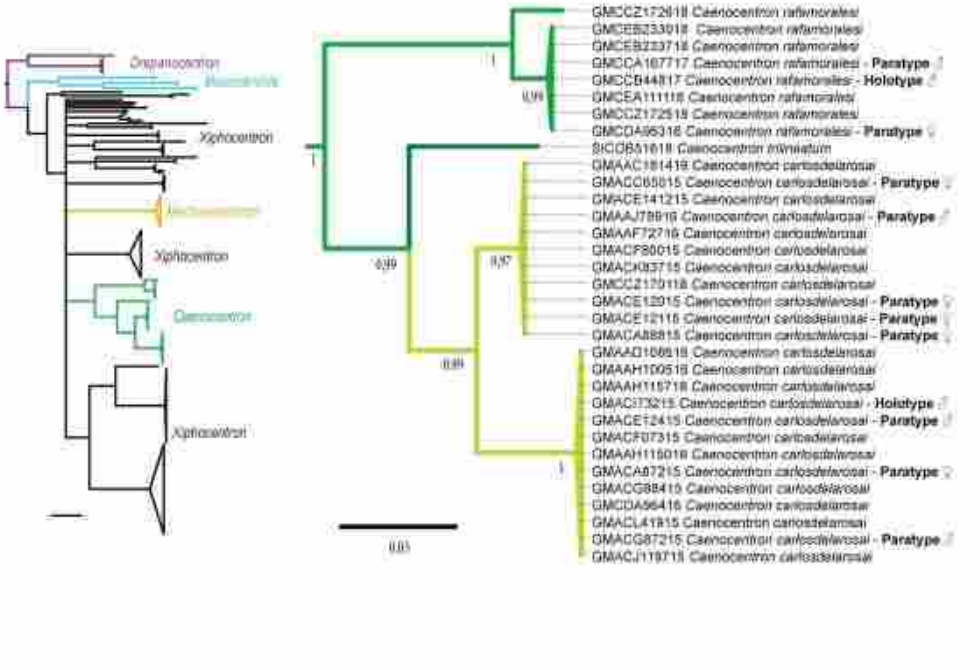

Figure 12. Bayesian analysis of COI sequences of Caenocentron carlosdelarosai sp. nov. and Caenocentron rafamoralesi sp. nov. and other xiphocentronids, showing clustering associating male and females of each species. Blue color = Caenocentron carlosdelarosai sp. nov.; yellow color = Caenocentron rafamoralesi sp. nov.; COI accession numbers are displayed in front of each specimen. Posterior probability values are displayed above each node.

256x192mm (300 x 300 DPI)

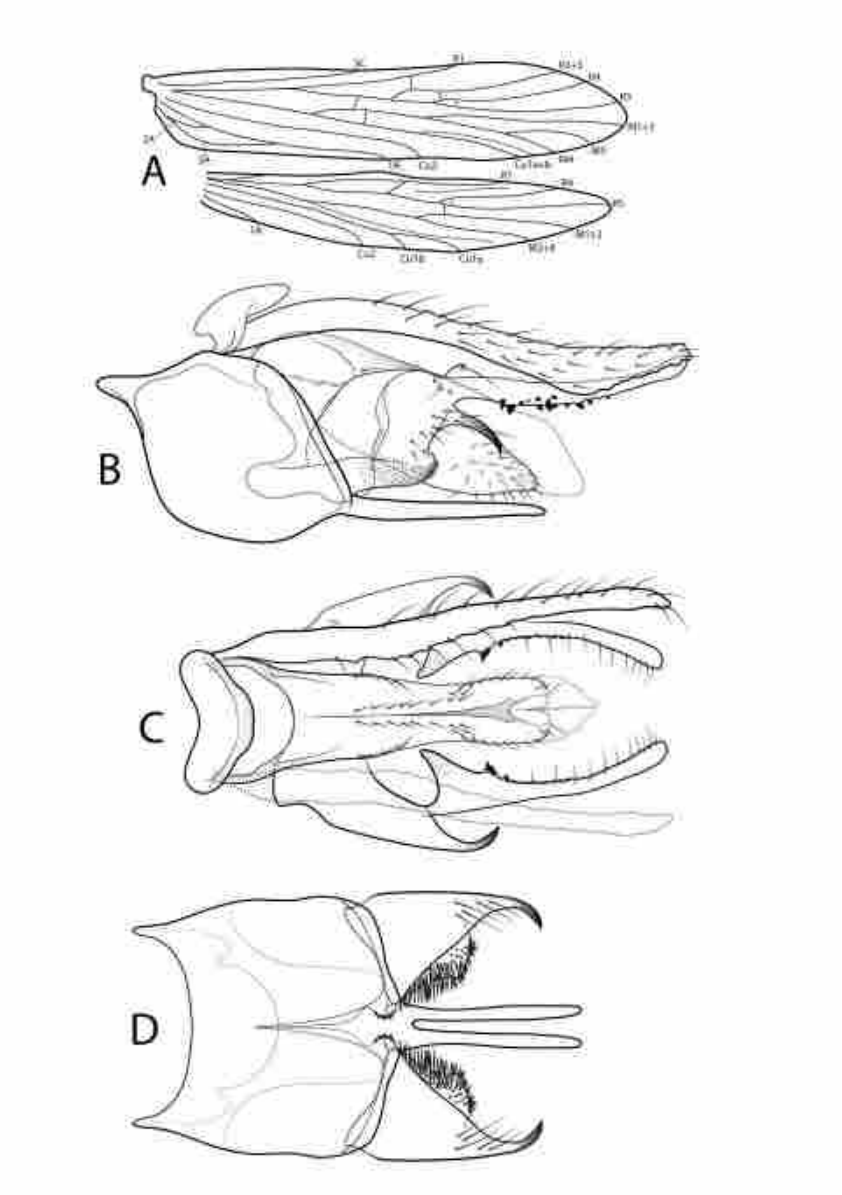

Figure 13. Caenocentron rafamoralesi sp. nov. A, Wing venation. Male genitalia B, lateral; C, dorsal; D, ventral.

316x450mm (300 x 300 DPI)

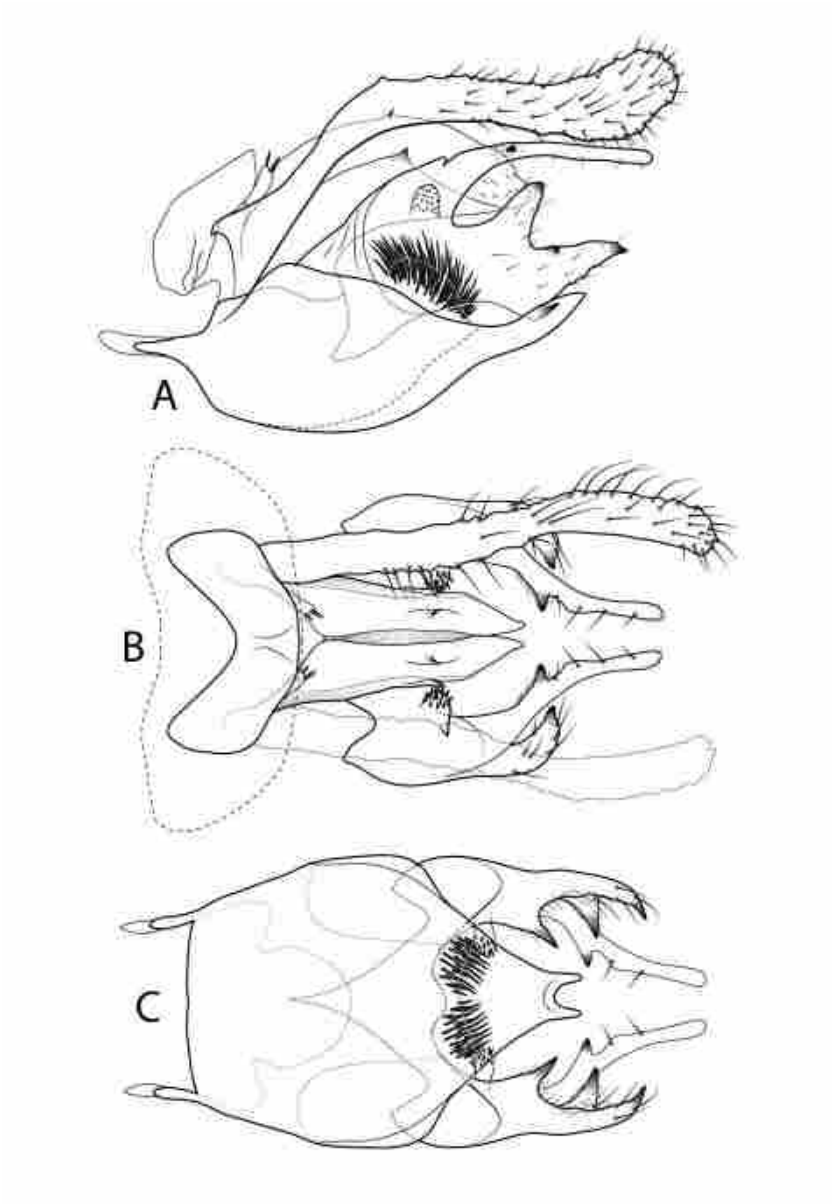

Figure 14. Caenocentron yavapai (Moulton & Stewart, 1997) male genitalia: A, lateral; B, dorsal; C, ventral.

316x458mm (300 x 300 DPI)

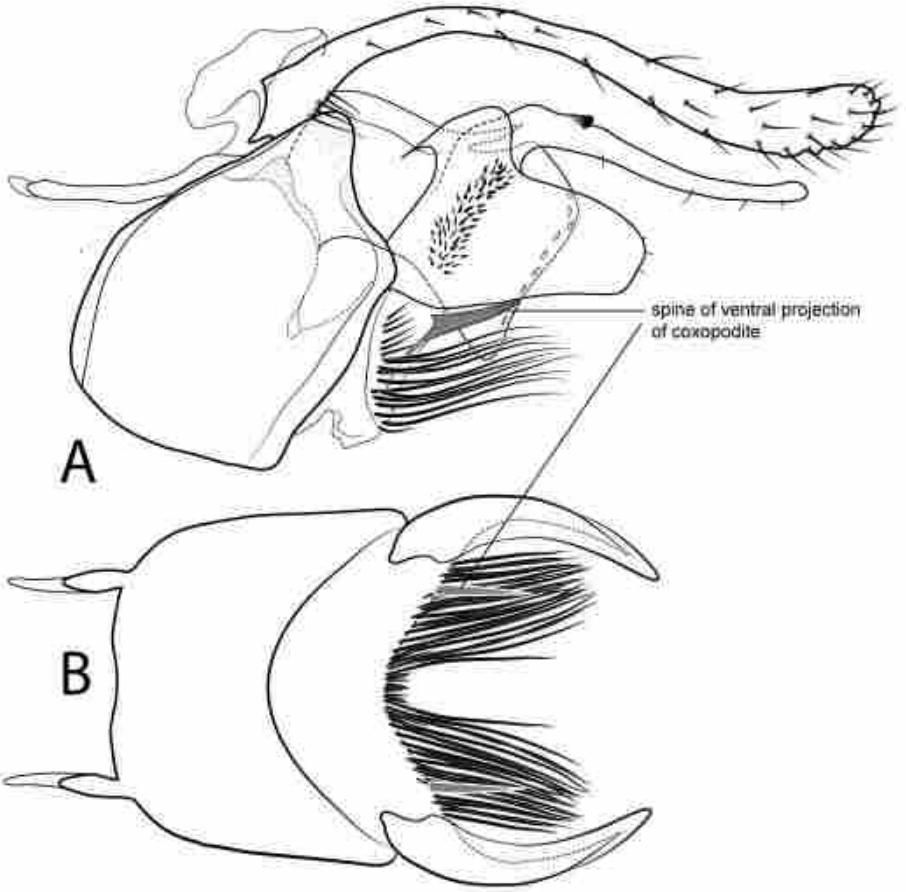

Figure 15. Caenocentron galesus (Schmid, 1982), male genitalia A, lateral; B, ventral.

269x309mm (300 x 300 DPI)

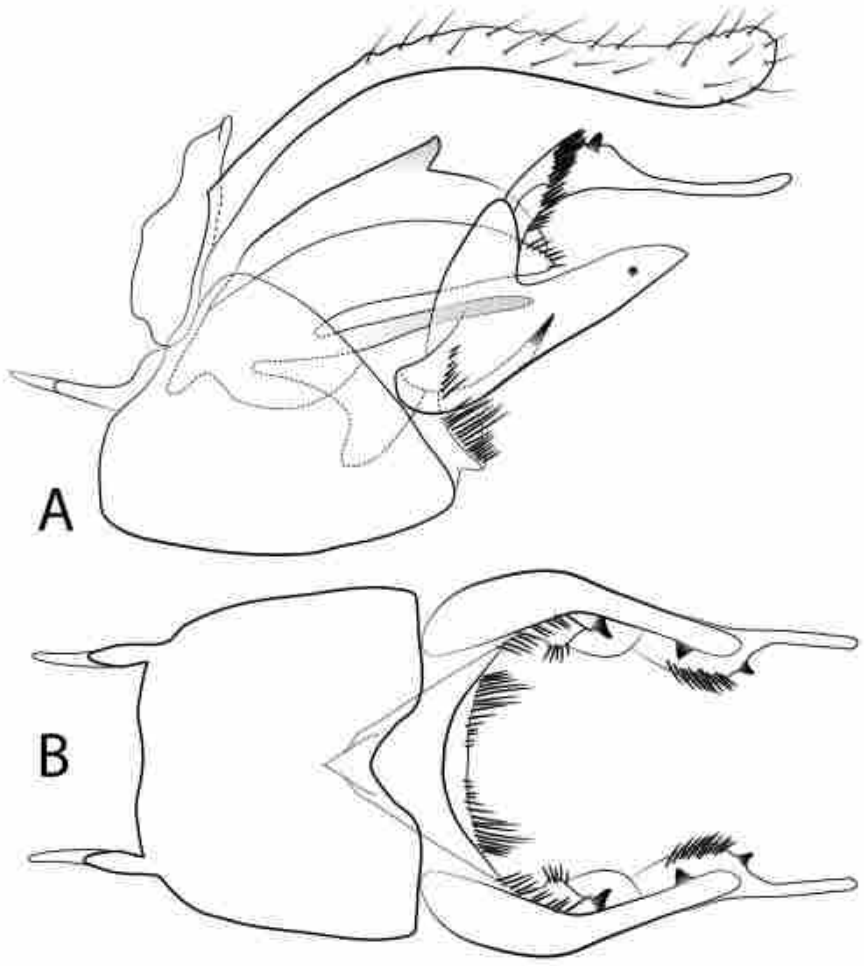

Figure 16. Caenocentron ideolus (Schmid, 1982), male genitalia: A, lateral; B, ventral.

269x309mm (300 x 300 DPI)

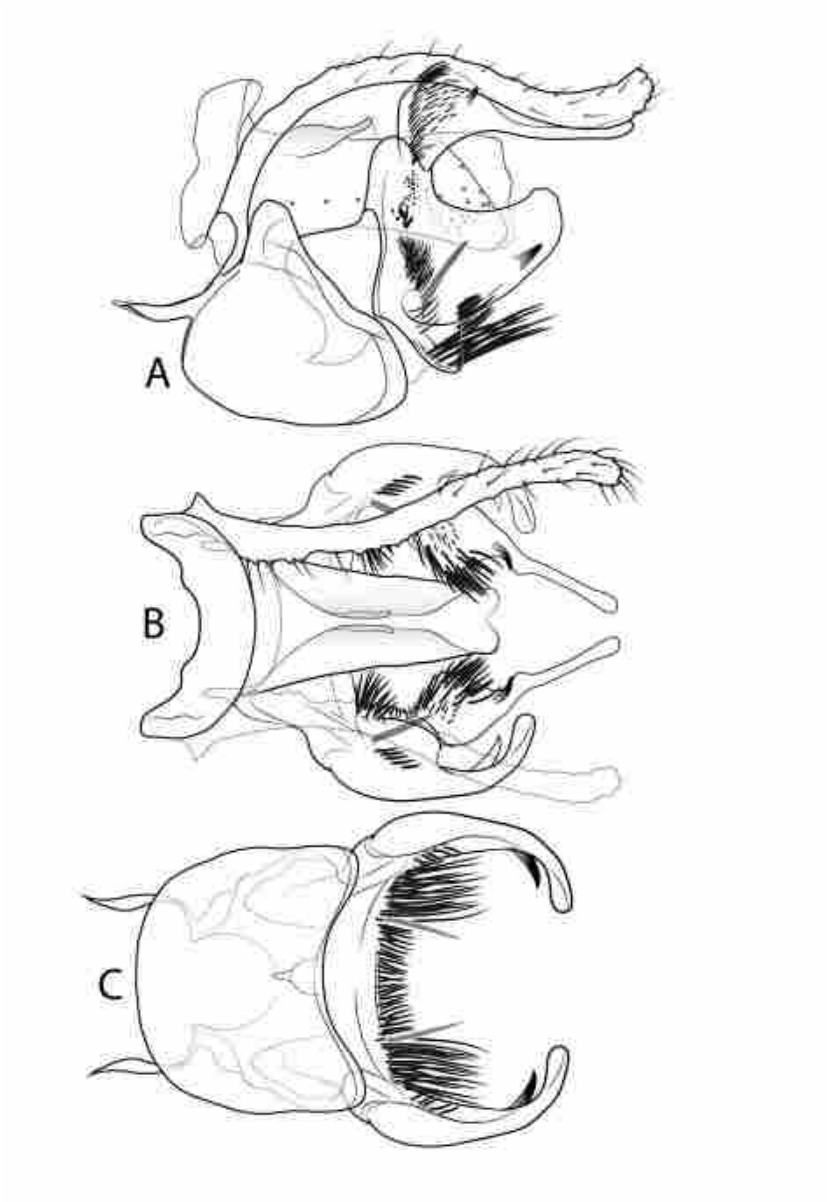

Figure 17. Caenocentron immaculatum (Flint, 1991), male genitalia: A, lateral; B, dorsal; C, ventral.

316x459mm (300 x 300 DPI)

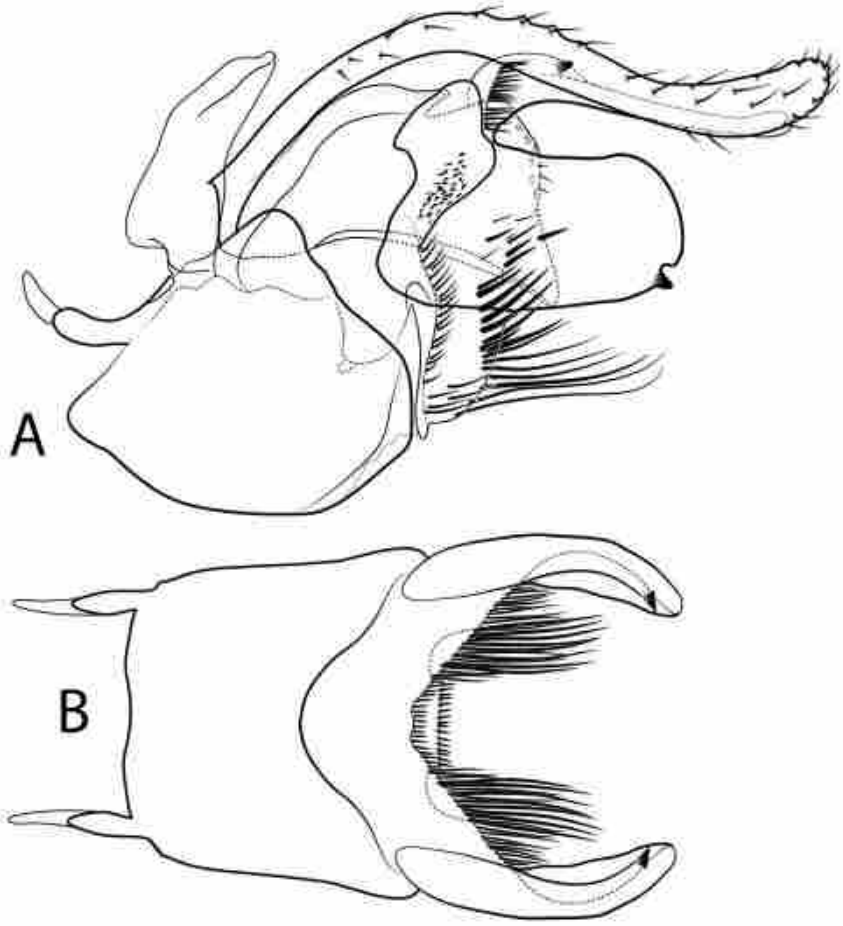

Figure 18. Caenocentron lausus (Schmid, 1982), male genitalia: A, lateral; B, ventral.

269x309mm (300 x 300 DPI)

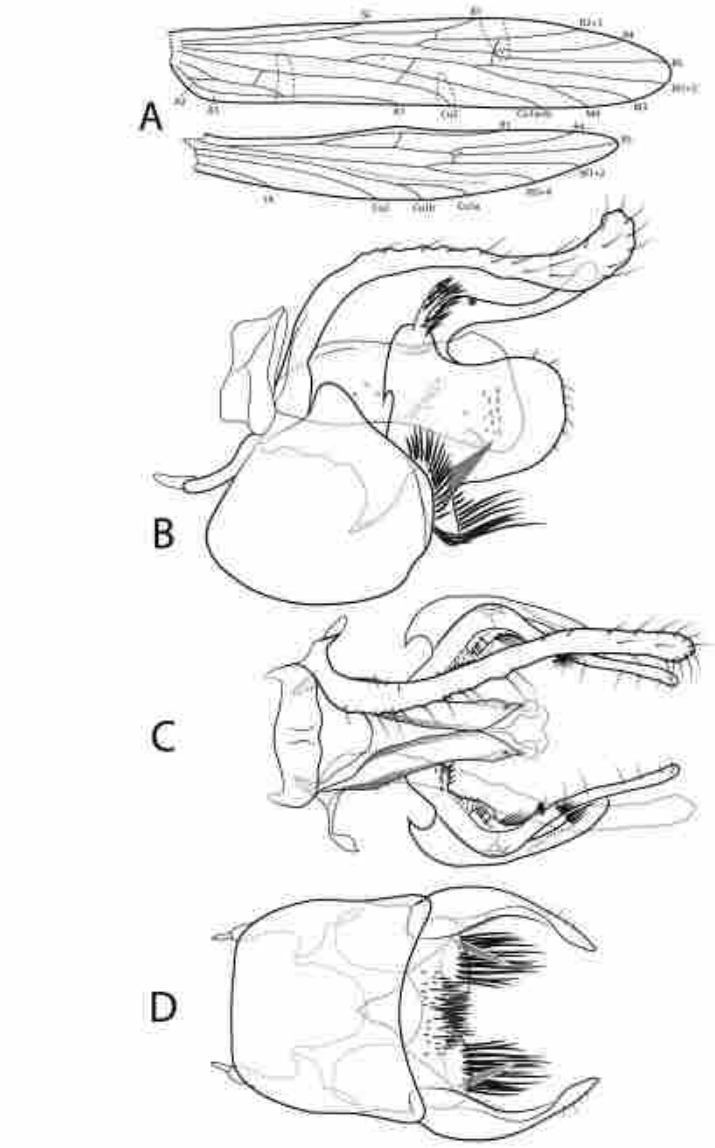

Figure 19. Caenocentron pallas (Schmid, 1982). A, Wing venation. Male genitália: B, lateral; C, dorsal; D, ventral.

316x464mm (300 x 300 DPI)

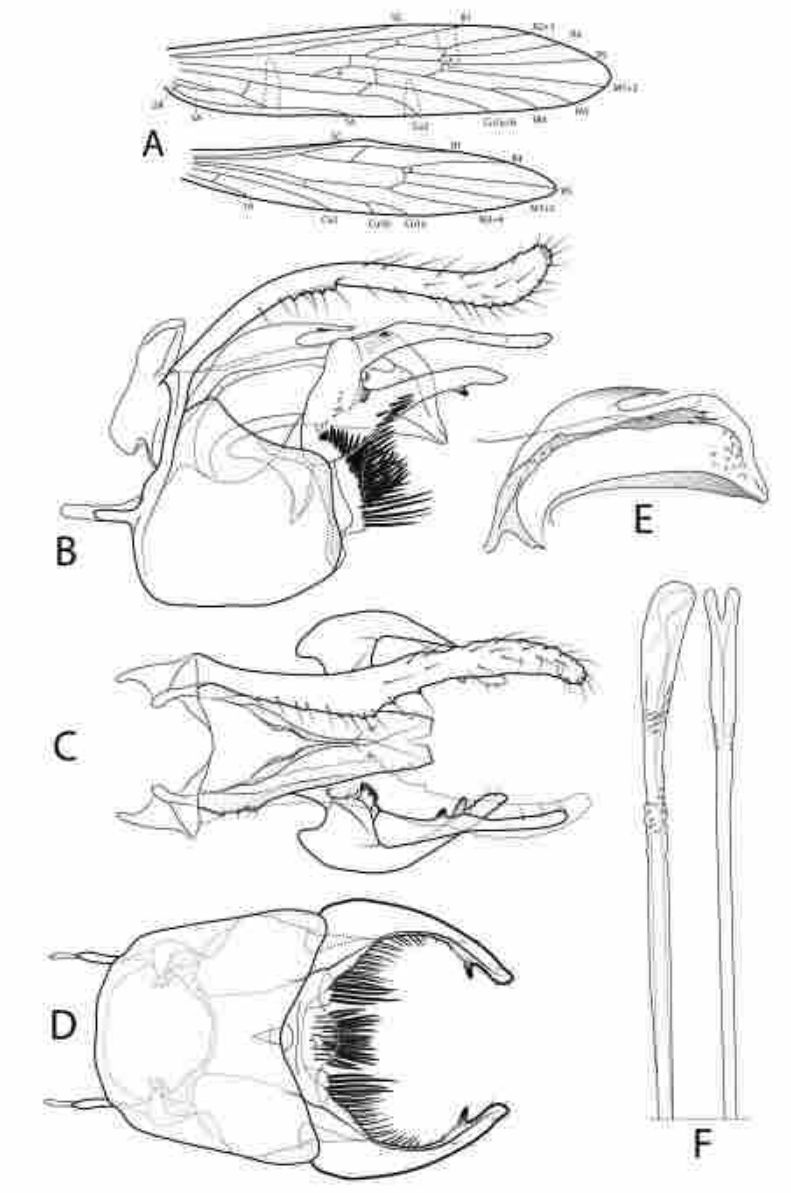

Figure 20. Caenocentron trilineatum (Mosely, 1934). A, Wing venation. Male genitalia: B, lateral; C, dorsal; D, ventral; E, detail paraproct lateral; F, phallus apex lateral and ventral, respectively.

316x480mm (300 x 300 DPI)

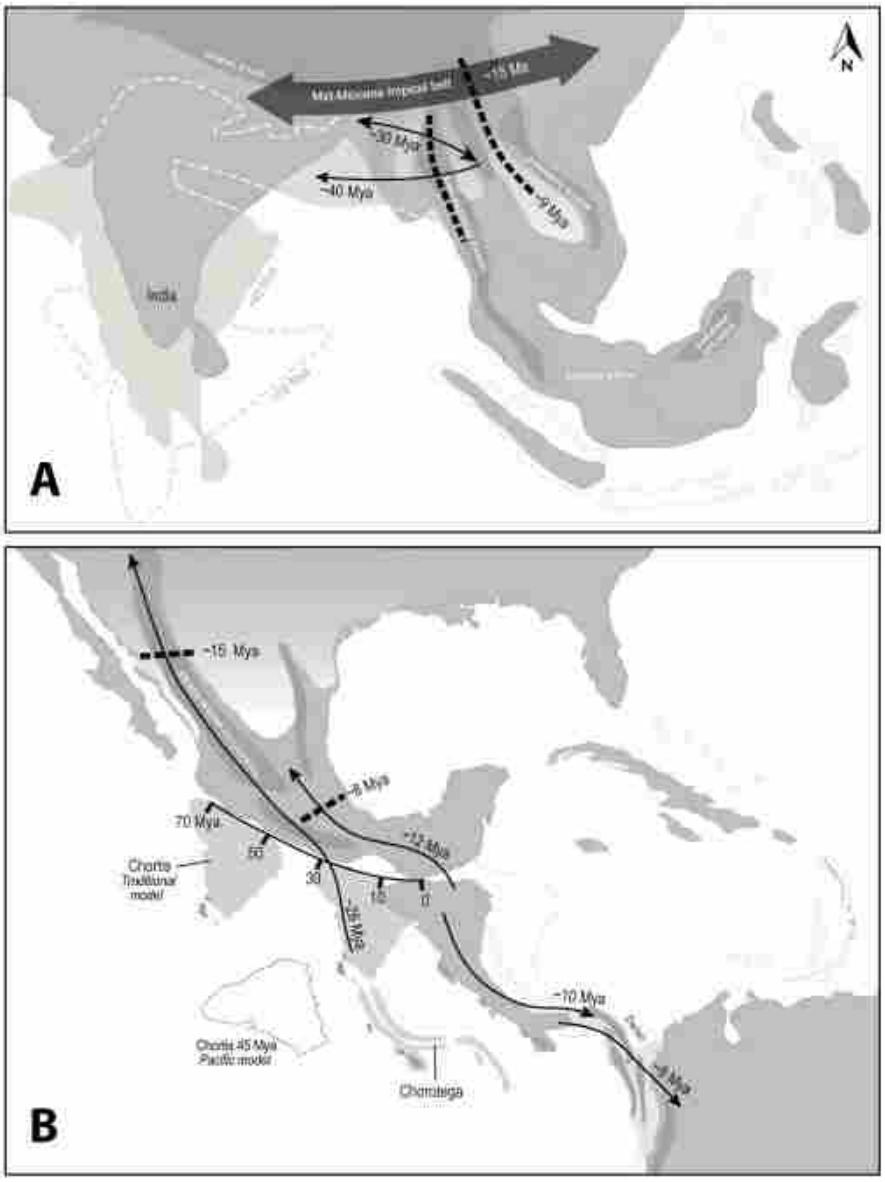

Figure 21. Paleogeography of Southeast Asia and Mesoamerica: A, Southeast Asia, showing the collision of Indian plate and Asia. B, Mesoamerica showing the southward movement of Chortis block. Dispersal and vicariant events with their respective mean ages are displayed as arrows and dotted lines, respectively. Montane regions are in dark gray. Whitish regions indicate progressive seasonal dry climates after the Middle Miocene. Paleogeographic reconstructions of Mesoamerica modified from Keppie & Zenteno (2005) and interpreted from evidences presented by Kirby et al. (2008), Coates et al. (2004) and Montes et al. (2012). Reconstructions of Southeast Asia modified after Morley (2018) and Gorin et al. (2020).

156x205mm (600 x 600 DPI)